# Quantity and distribution of methane entrapped in sediments of calcareous, Alpine glacier forefields

Biqing Zhu[1], Manuel Kübler[1], Melanie Ridoli[1], Daniel Breitenstein[1], Martin H. Schroth[1]

[1]Institute of Biogeochemistry and Pollutant Dynamics, ETH Zurich, Zurich, CH-8092, Switzerland

*Correspondence to*: Martin H. Schroth (martin.schroth@env.ethz.ch)

**Abstract.** Aside from many well-known sources, the greenhouse gas methane ($CH_4$) was recently discovered entrapped in sediments of Swiss Alpine glacier forefields derived from calcareous bedrock. A first study performed in one glacial catchment indicated that $CH_4$ was ubiquitous in sediments and rocks, and was largely of thermogenic origin. Here we present results of

10 a follow-up study, which aimed at (1) determining occurrence and origin of sediment-entrapped $CH_4$ in other calcareous glacier forefields across Switzerland, and (2) providing an inventory for this sediment-entrapped $CH_4$, i.e., determining contents and total mass of $CH_4$ present, and its spatial distribution within and between five different Swiss glacier forefields situated on calcareous formations of the Helvetic Nappes of the Central Alps.

Sediment and bedrock samples were collected at high spatial resolution from the forefields of Im Griess, Griessfirn,

15 Griessen, Wildstrubel, and Tsanfleuron glaciers, representing different geographic and geologic regions of the Helvetic Nappes. We performed geochemical analyses on gas extracted from sediments and rocks, including determination of $CH_4$ contents, stable carbon-isotope analyses ($\delta^{13}C_{CH4}$), and determination of gas-wetness ratios (ratio of $CH_4$ to ethane and propane contents). To estimate the total mass of $CH_4$ entrapped in glacier-forefield sediments, the total volume of sediment was determined based on measured forefield area and either literature values of mean sediment thickness or direct depth

20 measurements using electrical-resistivity tomography.

Methane was found in all sediments (0.08–73.81 µg $CH_4$ g$^{-1}$ dry weight) and most rocks (0.06–108.58 µg $CH_4$ g$^{-1}$) collected from the five glacier forefields, confirming that entrapped $CH_4$ is ubiquitous in these calcareous formations. Geochemical analyses further confirmed a thermogenic origin of the entrapped $CH_4$ (average $\delta^{13}C_{CH4}$ of sediment: -28.23 (± 3.42) ‰; average gas-wetness ratio: 75.2 (± 48.4)). Whereas sediment-entrapped $CH_4$ contents varied moderately within

25 individual forefields, we noted a large, significant difference in $CH_4$ content and total $CH_4$ mass (range: 200–3881 t $CH_4$) between glacier forefields at the regional scale. Lithology and tectonic setting within the Helvetic Nappes appeared to be dominant factors determining rock and sediment $CH_4$ contents. Overall, a substantial quantity of $CH_4$ was found to be entrapped in Swiss calcareous glacier forefields. Its potential release and subsequent fate in this environment is the subject of ongoing studies.

## 1 Introduction

The atmospheric concentration of the greenhouse gas methane ($CH_4$) has increased from pre-industrial values < 0.8 µL/L to a current global average of ~1.86 µL/L (Dlugokencky, 2018), indicating an imbalance in strength between $CH_4$ sources and sinks during this time period (Kirschke et al., 2013; Saunois et al., 2016; Ciais et al., 2013). Methane sources are commonly classified as either natural (e.g., wetlands, inland waters, geological sources (Etiope et al., 2008; Kirschke et al., 2013; Bastviken et al., 2011)), or, in case they result from human activity, anthropogenic (e.g., rice paddies, livestock husbandry, fossil fuels, and biomass burning (Bousquet et al., 2006; Kirschke et al., 2013; Johnson et al., 2002; Saunois et al., 2016)). An alternative way to categorize $CH_4$ sources is based upon the $CH_4$ production pathway: microbial, thermogenic, or abiotic (Conrad, 2009; Etiope and Sherwood Lollar, 2013; Joye, 2012; Whiticar, 1999). Microbial $CH_4$ is produced by methanogenic archaea (methanogens) under anoxic conditions and in the absence of energetically more favorable terminal electron acceptors as the final step of organic matter degradation (Conrad, 1996; Conrad, 2009; Denman et al., 2007). Conversely, thermogenic $CH_4$ is produced in sedimentary deposits under elevated temperatures and pressures during sediment diagenesis by thermal decomposition of organic matter (Etiope, 2012; Martini et al., 2003; Schoell, 1988). Together, microbial and thermogenic $CH_4$ are frequently referred to as biotic $CH_4$, as in both cases the initial substrates are of biological origin (Etiope and Sherwood Lollar, 2013). Finally, $CH_4$ can also be formed via inorganic chemical reactions in the Earth's crust and mantle, e.g., in serpentinized, ultramafic rocks, and is therefore referred to as abiotic $CH_4$ (Etiope and Sherwood Lollar, 2013; Etiope and Schoell, 2014; Etiope et al., 2018). Stable isotope analyses and/or analyses of gas composition are commonly employed to distinguish between microbial, thermogenic, and abiotic $CH_4$ origins (Etiope and Schoell, 2014; Whiticar, 1999; Milkov and Etiope, 2018; Schoell, 1988).

Accelerated melting of glaciers and ice sheets as a result of global warming (Haeberli et al., 2007; Paul et al., 2004; UNEP and WGMS, 2008) has prompted intense research activities in glacial environments, including investigations on their role in the turnover of greenhouse gases. Several studies have identified subglacial environments as habitats for methanogens, and consequently as a potentially important $CH_4$ source (Wadham et al., 2012; Wadham et al., 2013; Christner et al., 2012; Souchez et al., 1995; Stibal et al., 2012). Methane emissions from these locations have recently been confirmed and quantified in field measurements (Burns et al., 2018; Christiansen and Jørgensen, 2018; Lamarche-Gagnon et al., 2019). Conversely, other studies provided evidence that aerated glacier-forefield sediments can act as a sink for atmospheric $CH_4$ (Chiri et al., 2015; Nauer et al., 2012; Bárcena et al., 2010; Hofmann et al., 2013). This function is mediated by a group of aerobic methane-oxidizing bacteria (MOB), which catalyze $CH_4$ oxidation at near-atmospheric concentrations (Curry, 2009; Zhuang et al., 2013; Dunfield, 2007). The strength of this $CH_4$ sink appears to vary between different glacier-forefield landforms, and increase with sediment age (Bárcena et al., 2010; Chiri et al., 2017; Hofmann et al., 2013). In this context, sediment age refers to the number of years sediment has been exposed to the atmosphere following glacier retreat. Note that both terms, sediment age and landform, serve as proxies for all edaphic variations present in these sediments at different locations within the glacier forefield. We will adopt this convention and use the terms sediment age and landform in this fashion throughout this paper.

An alternative potential $CH_4$ source was recently detected in sediments of Swiss glacier forefields, in particular in those derived from calcareous bedrock (Nauer et al., 2012). Subsequent laboratory experiments revealed that $CH_4$ was released from glacier-forefield sediments upon mechanical impact and during acidification (Nauer et al., 2014). In a recent study focusing on one particular Swiss glacial catchment (Wildstrubel catchment, Canton Valais), we established that entrapped $CH_4$ was present in nearly all sediment and bedrock samples collected throughout this catchment, but that $CH_4$ contents exhibited substantial variation between sampling locations (Zhu et al., 2018). We also provided robust evidence based on stable-isotope and other geochemical data that $CH_4$ entrapped in sediment and bedrock samples was predominantly of thermogenic origin, and that microbial $CH_4$ production was likely of minor importance at this site. However, as the focus of that study was on the occurrence and origin of entrapped $CH_4$ in different regions of the catchment, the number of samples collected was insufficient to rigorously assess spatial distribution and total quantity (here defined in terms of content, i.e., concentration, and total mass) of entrapped $CH_4$ within the forefield sediments (Zhu et al., 2018). Yet, to better characterize this potential $CH_4$ source, it is important to assess its spatial distribution and total quantity, particularly in glacier-forefield sediments, as we expect the potential for $CH_4$ release from these sediments to far exceed that from large bedrock surfaces due to the much higher specific surface area of the former (André et al., 2009; Michel and Courard, 2014). Moreover, as calcareous glacier-forefield sediments throughout the Swiss Alps are of similar origin (Weissert and Stössel, 2015), sediment-entrapped $CH_4$ may be a feature common to most if not all Swiss glacier forefields derived from calcareous bedrock. Whereas this hypothesis remains to be tested, its confirmation would greatly increase the magnitude of this potential $CH_4$ source.

Therefore, the overall goal of this study was to extend the work of Zhu et al. (2018) to other calcareous glacier forefields located in different regions of the Swiss Alps, and to assess the distribution of entrapped $CH_4$ contents within and compare total mass of entrapped $CH_4$ between all sampled glacier forefields. Specific objectives included to (1) test occurrence and origin of sediment-entrapped $CH_4$ in four additional calcareous glacier forefields. Furthermore, we wanted to (2) assess the spatial distribution of sediment-entrapped $CH_4$ contents in detail within one glacier forefield, testing for dependencies on sediment depth, sediment age, and glacier-forefield landforms, and based on the results obtained to (3) efficiently sample sediments of the other glacier forefields to quantify contents and total mass of sediment-entrapped $CH_4$. Finally, we wanted to (4) upscale these results and derive a first estimate of the total mass of sediment-entrapped $CH_4$ contained in all Swiss glacier forefields situated on calcareous bedrock.

## 2 Methods

### 2.1 Field sites and field-work stages

Field work was conducted in five different glacier forefields: Im Griess (IMG), Griessfirn (GRF), and Griessen (GRI) glaciers located in Central Switzerland in Cantons Uri (IMG, GRF) and Obwalden (GRI), and Tsanfleuron (TSA) and the previously investigated Wildstrubel (WIL, Zhu et al. (2018)) glaciers located in Canton Valais (Figs. 1 and S1). These forefields were selected for two main reasons. Foremost, their sediments are mainly derived from calcareous bedrocks of the Helvetic Nappes

(green shaded area in Fig. 1), which consist of a series of nappes (sheets of thrusted rocks) largely composed of Mesozoic limestones, shales, and marls of Jurassic to Eocene age (Pfiffner, 2014; Weissert and Stössel, 2015). They were originally deposited on the shallow northern shelf of the ancient Alpine Tethys Ocean (Weissert & Mohr, 1996), and subsequently deformed, folded, and stacked on top of each other during Alpine orogeny (Herwegh and Pfiffner, 2005). Whereas individual nappes within the Helvetic Nappe system therefore share a similar origin, lithology and tectonic settings between individual nappes can be quite diverse (Weissert and Stössel, 2015). This was suggested to be a dominant factor determining rock $CH_4$ contents in the WIL catchment (Zhu et al., 2018). Consequently, we chose to investigate glacier forefields distant from one another (e.g., distance TSA to IMG ~136 km), for which sediments are derived from different nappes, but also glacier forefields in close proximity to each other (e.g., distance IMG to GRF ~3.8 km; TSA to WIL ~24 km), for which sediments are derived, at least in part, from the same nappe. A second important reason for selection was that all five glacier forefields are relatively easy to access, facilitating sample collection and transport to the laboratory.

We conducted our field work in two stages. During stage I in summer 2016, we performed a detailed investigation on the spatial distribution of sediment-entrapped $CH_4$ within a designated sampling zone at the GRF glacier forefield, using high spatial-resolution sampling to determine variations in entrapped $CH_4$ contents in relation to sediment depth, sediment age, and glacier-forefield landforms. The GRF forefield was chosen for this purpose mainly because it features well-defined sediment-age classes and well-developed, clearly distinguishable landforms within a previously discretized and characterized sampling zone (Chiri et al., 2015; Chiri et al., 2017). We also conducted measurements of sediment thickness (distance between the ground surface and the underlying bedrock) to estimate sediment volumes and thus the total mass of entrapped $CH_4$ present in these sediments. Results of the GRF field work were then used to adapt our sampling strategies for field-work stage II performed in summer 2017, to quantify contents and total mass of sediment-entrapped $CH_4$ in the IMG, GRI, TSA, and WIL glacier forefields. During both field-work stages, selected sediment and rock samples were used to identify the origin of the entrapped $CH_4$ based on $CH_4$ stable carbon-isotope analyses and analyses of entrapped gas composition (see below).

### 2.1.1 Field-work stage I (GRF glacier forefield)

Sampling and measurements during stage I in the GRF forefield was conducted in three steps. First we tested the effect of sediment depth, then the effects of sediment age and glacier-forefield landforms on entrapped $CH_4$ contents. Finally, we estimated the total mass of sediment-entrapped $CH_4$ based on measured $CH_4$ content, sediment thickness, and sediment-covered area.

To study the effect of sediment depth on entrapped $CH_4$ contents, we implemented a randomized design, selecting 14 random locations within our sampling zone (not shown). We collected a total of 52 sediment samples (each ~500 g) by excavation from depths ranging from 20 to 70 cm below ground surface. All sediment samples were stored in clean plastic bags, transferred to the laboratory, and kept in the dark at 4 °C before further treatment. Following the extraction of entrapped gas and subsequent quantification of $CH_4$ contents in sediment samples (see below), the effect of sediment depth on entrapped

CH$_4$ contents was studied using a one-way ANOVA. The result of this analysis was then used to adapt the sampling scheme for the following step.

To study the effect of sediment age and glacier-forefield landforms on entrapped CH$_4$ contents, we implemented a randomized block-sampling design. We first divided the GRF sampling zone into nine blocks (a combination of three sediment-age classes and three landforms, Fig. 2a), using the spatial discretization of Chiri et al. (2017). The three sediment-age classes were: A (0–20 yr), B (20–50 yr) and C (50–100 yr). The three forefield landforms at GRF were floodplain, terrace, and sandhills. A floodplain refers to the frequently flooded area in the immediate vicinity of the glacial stream, which commonly consists of sediments of fine particle size (mostly silt) and a lack of vegetation. A terrace refers to an elevated, previously flooded area, i.e. a former floodplain, usually featuring some vegetation coverage. Finally, sandhills consist of un-oriented, hummocky glacial-debris deposits, typically featuring poorly sorted, well-aerated sediments of sandy loam to sandy clay-loam texture. We collected a total of 78 sediment samples (each ~500 g) by excavation from a depth of 20 cm below ground surface, with 8–12 samples collected at random locations from within each block (Fig. 2a). The sampling depth of 20 cm below ground surface was chosen based on our results from the previous step. Following laboratory analyses (see below), the impact of sediment age and landforms on entrapped CH$_4$ contents was studied using a two-way ANOVA.

In addition to sediments, we also collected a total of 17 bedrock samples from outcrops and large boulders within the GRF glacier forefield. These samples were used to determine the CH$_4$ content of the parent material (Zhu et al., 2018). All bedrock samples were stored in plastic bags, transferred to the laboratory, and stored in dark at 4 °C before further treatment.

Estimation of the total mass of CH$_4$ entrapped in glacier-forefield sediments also requires information on sediment thickness. For the GRF sampling zone we employed the electrical resistivity tomography (ERT) method (e.g., Kneisel, 2006; Reynolds, 1997; Scapozza et al., 2011). Five two-dimensional, vertical ERT profiles (ERT1–ERT5) were measured during two field campaigns, covering the three sediment-age classes and the three landforms (Fig. 2b). Two profiles were measured parallel to the glacier stream (ERT2 and ERT5), and three perpendicular to the glacier stream (ERT1, 3, and 4). For each profile, 48 stainless-steel electrodes (30 cm long, 1.2 cm dia.) were hammered into the sediment to a depth of ~15 cm and connected to two 24-core copper cables, which were linked to the ERT instrument (SYSCAL Pro; Iris Instruments, Orléans, France) at the profile's midpoint. To improve electrical coupling of the electrodes with the skeleton-rich glacier-forefield sediments, water-soaked sponges were positioned at the sediment surface surrounding each electrode. Profile ERT1 was measured with an electrode interspacing of 2.5 m (total profile length 120 m), the other four with 5 m distance between the electrodes (240 m profile length). Using a so-called Wenner-Schlumberger configuration (Loke, 2001), an electrical current was sent to the subsurface using a pair of electrodes. The voltage difference measured across the other pairs of electrodes was used to calculate the electrical resistivity of the subsurface. To infer the location of the sediment-bedrock interface, inversion of apparent resistivities was performed using the 2-D program RES2DINV (Loke and Barker, 1996). The average sediment thickness and its uncertainty within the GRF forefield was then analyzed in R. Electrical resistivities >2000 Ωm were considered indicative of solid bedrock, whereas resistivities < 2000 Ωm were considered indicative of unconsolidated sediment

160 (Kneisel, 2006; Reynolds, 1997). Portions of the ERT profiles, for which the sediment-bedrock interface could not be detected, were omitted from further analyses.

### 2.1.2 Field-work stage II (IMG, GRI, WIL, and TSA glacier forefields)

During stage II, we collected a total of 111 sediment samples at 20 cm depth, 25 samples from IMG, 25 from GRI, 33 from WIL, and 28 from TSA glacier forefields (sampling locations shown in Fig. 3). Based on results obtained during field-work
165 stage I, and given that glacier-forefield landforms were much less prominent at IMG, GRI, WIL, and TSA, we divided each of the four forefields into six blocks, and collected four to eight sediment samples (each ~500 g) from each block at random locations. We also collected 55 bedrock samples from outcrops and boulders; 13 from IMG, 14 from GRI, 12 from WIL, and 16 from TSA glacier forefields (locations also shown in Fig. 3).

### 2.2 Laboratory procedures

170 ### 2.2.1 Extraction of entrapped gas

We extracted entrapped gas from sediments and rocks using the acidification method described in Nauer et al. (2014) and Zhu et al. (2018). Before acid treatment, sediments were sieved with a clean 20 mm mesh sieve. Particles >20 mm were excluded from subsequent analyses. For each sample, ~3–5 g of sediment was weighed and transferred into a 117 mL serum bottle, sealed with a butyl rubber stopper and crimped with an aluminum cap. The vial's headspace was then flushed with $N_2$ gas.
175 Thereafter, 5 mL deionized water was added into the vial, followed by ~50 mL of 6 N HCl to dissolve carbonate minerals. The headspace of each vial was connected to one or multiple 1 L gas bags (Tesseraux GmbH, Bürstadt, Germany). Sediment samples released large amounts of gas immediately after the acid was added. When bubbling stopped, an additional 2 mL 6N HCl was added to each vial to confirm that the carbonate minerals were fully dissolved. Full dissolution of all carbonate minerals took ~4 h. After gas extraction, ~200 mL of gas were removed from the gasbags with syringes and stored in glass
180 vials for further analysis. The total volume of gas remaining in gas bags was measured with a mass-flow meter (Bronkhorst, Reinach, Switzerland). Rocks were first hammered or sawed into ~1 cm diameter fragments and then dissolved in the same way as sediments. Initial tests, in which we compared hammering with sawing to obtain rock fragments both from the surface and from the core of larger rocks, showed insignificant effects on the fragments' entrapped $CH_4$ contents and other geochemical parameters. As the duration of the respective mechanical treatment varied greatly between the collected fragments, we consider
185 this as evidence that neither hammering nor sawing had an adverse effect on measured geochemical parameters.

### 2.2.2 Quantification of methane, ethane, and propane

Concentrations of $CH_4$ were measured with a gas chromatograph equipped with a flame-ionization detector (GC-FID; Trace GC Ultra, Thermo Electron, Rodano, Italy) and a Porapak N100/120 column. The column-oven temperature was 30 °C, runtime was 36 s. Nitrogen carrier-gas flow was set to 26 mL/min. The FID was operated at 150 °C in high sensitivity mode.

190     Concentrations of ethane ($C_2H_6$) and propane ($C_3H_8$) were quantified in selected gas samples using the same GC-FID system, but with oven temperature at 40 °C for 2 min, an increase to 140 °C at a rate of 25 °C/min, and constant oven temperature of 140 °C for another 9 min. Gas contents were calculated as the mass of $CH_4$, $C_2H_6$, and $C_3H_8$ released during acidification, normalized to the dry weight of the sample. The dry weight of sediments was determined by oven-drying of subsamples at 60 °C for 72 h. Computed entrapped gas contents $C_{CH4}$, $C_{C2H6}$, and $C_{C3H8}$ were subsequently used to calculate the gas-wetness

195     ratio as $C_{CH4}/(C_{C2H6} + C_{C3H8})$ (Jackson et al., 2013), a commonly used indicator of $CH_4$ origin (a value >1,000 is considered evidence for microbial $CH_4$, whereas a value <<1,000 is considered indicative of thermogenic $CH_4$ (Rowe and Muehlenbachs, 1999)).

### 2.2.3 Stable carbon-isotope analysis of entrapped methane

    A total of 31 sediment and bedrock samples from the five glacier forefields were selected for stable carbon-isotope analysis of

200     entrapped $CH_4$ ($\delta^{13}C_{CH4}$). To determine $\delta^{13}C_{CH4}$ we used a modified acidification protocol for gas extraction, which consisted of flushing the vials' headspace with He instead of $N_2$ to remove ambient air. Gas released during the acidification treatment was passed through two 1 M NaOH solutions to remove the majority of $CO_2$, an Ascarite trap to remove final traces of $CO_2$, a Drierite trap to remove $H_2O$ vapor, and a 1 M $ZnCl_2$ trap to remove potential $H_2S$ (all chemicals from Sigma Aldrich, Buchs, Switzerland). The purified gas samples were subsequently analyzed by GC-IRMS (Isoprime, Elementar Ltd., Stockport, UK).

205 **2.3 Estimation of total mass of $CH_4$ entrapped in glacier-forefield sediments**

### 2.3.1 Estimation of entrapped $CH_4$ mass for the GRF sampling zone

    The mass of $CH_4$ ($m_{CH4}$) entrapped in a specific volume of porous sediment may be calculated using:

$$m_{CH4} = C_{CH4}\, \rho_{sed} \left[ A_{sed}\, T_{sed} \left(1 - \theta_{t,sed}\right) \right] \tag{1}$$

    where $C_{CH4}$ is sediment-entrapped $CH_4$ content (mass of $CH_4$ per mass of sediment), $\rho_{sed}$ is sediment-particle density, $A_{sed}$ and

210     $T_{sed}$ are sediment-covered area and sediment thickness in the glacier forefield, and $\theta_{t,sed}$ is total inter-particle sediment porosity, hereafter referred to as sediment porosity. To determine $m_{CH4}$ for the GRF sampling zone, we applied Eq. (1) separately to each landform, but also used averaged values for entrapped $CH_4$ contents (from laboratory analyses), sediment thickness (from ERT field measurements), and sediment-covered area estimated from aerial maps (https://map.geo.admin.ch). In Eq. (1), the term in brackets represents the sediment's solid volume. To compute the latter, we assumed a mean $\overline{\theta}_{t,sed} = 0.42 \pm 0.02$, as

215     determined for this site by Nauer et al. (2012). To convert solid volume to sediment mass, a mean value of $\overline{\rho}_{sed} = 2.71 \pm 0.15$ g cm$^{-3}$ was used, as derived by Daly (1935) from measurements of a variety of calcite rock samples.

The total uncertainty in the estimated mean CH$_4$ mass $\bar{m}_{CH4}$, expressed as standard error (SE) of the mean ($\sigma_{\bar{m}_{CH4}}$), was computed using:

$$\sigma_{\bar{m}_{CH4}} = \bar{m}_{CH4} \sqrt{\left(\frac{\sigma_{\bar{C}_{CH4}}}{\bar{C}_{CH4}}\right)^2 + \left(\frac{\sigma_{\bar{\rho}_{sed}}}{\bar{\rho}_{sed}}\right)^2 + \left(\frac{\sigma_{\bar{A}_{sed}}}{\bar{A}_{sed}}\right)^2 + \left(\frac{\sigma_{\bar{T}_{sed}}}{\bar{T}_{sed}}\right)^2 + \left(\frac{\sigma_{\bar{\theta}_{t,sed}}}{\bar{\theta}_{t,sed}}\right)^2} \tag{2}$$

220    where $\sigma_{\bar{x}}$ represents the SE associated with any parameter's mean value $\bar{x}$. The individual contribution of any parameter $x$ (*frac$_x$*, in %) to the total uncertainty in $\bar{m}_{CH4}$ was then computed using:

$$frac_x = \left(\frac{\bar{m}_{CH4}}{\sigma_{\bar{m}_{CH4}}}\left(\frac{\sigma_{\bar{x}}}{\bar{x}}\right)\right)^2 \times 100 \tag{3}$$

We note that throughout this manuscript SE values (reported as $\bar{x} \pm \sigma_{\bar{x}}$) are used as a measure of uncertainty of any parameter's mean value $\bar{x}$, whereas standard deviations (SD, reported as $\bar{x}(\pm \sigma_x)$) are used as a measure of general parameter 225    variability.

**2.3.2 Estimation of entrapped CH$_4$ mass for the five glacier forefields (IMG, GRF, GRI, WIL, TSA)**

To compute total mass and associated uncertainty of sediment-entrapped CH$_4$ for all five glacier forefields, we employed Eqs. (1) and (2), but with partially modified parameters. For $C_{CH4}$ we used mean values of sediment-entrapped CH$_4$ contents determined for each glacier forefield. In addition we determined mean values $\bar{A}_{sed}$ from estimates of the maximum and 230    minimum extents of sediment-covered area within each glacier forefield. As maximum we used the areas exposed as a result of glacier retreat since the last glacial maximum (Little Ice Age, ~1850). The latter was estimated from the difference in glacial extent as taken from the most current (2018) and historic (~1850) topographic maps (Swisstopo; https://map.geo.admin.ch; Fig. S2). Minimum areas were directly estimated from the 2018 aerial maps. Also, data on sediment thickness was unavailable for the IMG, GRI, WIL, and TSA glacier forefields, as well as for the GRF forefield outside of the designated sampling zone. 235    We therefore used the average value of $T_{sed}$ = 10.0 ± 3.0 m obtained from our ERT measurements in the GRF sampling zone (see below) as an average $T_{sed}$ for all five glacier forefields. We note that our average $T_{sed}$ value agrees well with previous measurements performed in another Swiss glacier forefield, in which $T_{sed}$ ~8 m was obtained by borehole drilling (Kneisel and Kääb, 2007). Finally, we used values of $\bar{\theta}_{t,sed}$ for GRF, GRI, and WIL forefields as determined for these sites by Nauer et al. (2012). As such values were unavailable for the IMG and TSA forefields, we used a value of $\bar{\theta}_{t,sed}$ = 0.44 ± 0.05 for the latter, 240    averaged from data reported for five calcareous glacier forefields (Nauer et al., 2012).

### 2.3.3 Estimation of entrapped CH$_4$ mass for sediments in all Swiss glacier forefields derived from calcareous bedrock

We again used Eq. (1) and (2) to upscale results and to compute a first estimate of the total mass of sediment-entrapped CH$_4$ contained in all Swiss glacier forefields derived from calcareous bedrock. In this case, we used the mean $\overline{C}_{CH4}$ of the five glacier forefields. Calcareous glacier-forefield surface area in Switzerland ($A_{sed}$ in Eq. (1)) was estimated from available data on the decrease in glaciated area in the Swiss Alps between the Little Ice Age (~1850; Zemp et al. (2008)) and the year 2010 (Fischer et al., 2014), together with an estimate of the fraction of calcareous bedrock area to the total area of the Swiss Alps taken from the Tectonic Map of Switzerland 1:500.000 (Federal Office of Topography, swisstopo). Mean values for $\rho_{sed}$, $T_{sed}$, and $\theta_{t,sed}$ were used as described above.

## 3 Results

### 3.1 Geochemistry of gas entrapped in sediment and bedrock samples

Of the 271 sediment samples from the five glacier forefields we analyzed 256 samples for entrapped CH$_4$ contents. All analyzed sediments contained detectable amounts of CH$_4$ ranging from 0.08 to 73.81 µg CH$_4$ g$^{-1}$ dry weight (d.w.; Fig. 3), with an average of 14.9 ($\pm$ 17.0) µg CH$_4$ g$^{-1}$ d.w.. Gas released from 225 samples was analyzed for C$_2$H$_6$ and C$_3$H$_8$ contents, of which 215 contained detectable amounts of C$_2$H$_6$ ranging from 0.002 to 1.67 µg C$_2$H$_6$ g$^{-1}$ d.w., with an average of 0.25 ($\pm$ 0.32) µg C$_2$H$_6$ g$^{-1}$ d.w.. In addition, 146 out of 225 samples contained detectable amounts of C$_3$H$_8$ ranging from 0.001 to 0.82 µg C$_3$H$_8$ g$^{-1}$ d.w., with an average of 0.11 ($\pm$ 0.15) µg C$_3$H$_8$ g$^{-1}$ d.w. (not shown).

The average gas-wetness ratio for all sediment samples was 75.2 ($\pm$ 48.4), and the average $\delta^{13}C_{CH4}$ was -28.23 ($\pm$ 3.42) ‰. Plotting $\delta^{13}C_{CH4}$ values vs. gas-wetness ratios in a so-called Bernard diagram (Fig. 4; Bernard et al. (1978)) indicated a thermogenic origin for sediment-entrapped CH$_4$, derived from ancient terrestrial or marine organic matter (kerogen types III and II, Fig. 4). Although CH$_4$ extracted from sediments collected in the IMG glacier forefield showed a higher variability in gas-wetness ratios than CH$_4$ extracted from sediments of other glacier forefields, it still fell into the same origin type in the Bernard diagram.

All 72 bedrock samples were analyzed for CH$_4$ content, and 64 contained detectable amounts of CH$_4$ ranging from 0.06 to 108.58 µg CH$_4$ g$^{-1}$, with an average of 11.4 ($\pm$ 20.0) µg CH$_4$ g$^{-1}$ (Fig. 3). The average $\delta^{13}C_{CH4}$ value of -29.21 ($\pm$ 2.77) ‰ was similar to that of sediment-entrapped CH$_4$. Likewise, the average gas-wetness ratio of gas extracted from rocks was 78.45 ($\pm$ 121.84), similar in value but with higher variability than gas-wetness ratios for sediment-entrapped CH$_4$ (Fig. 4). Together, these data suggest a common, thermogenic origin of entrapped CH$_4$ in sediments and rocks, with little apparent alteration from physical/chemical weathering. Moreover, our data suggest that entrapped CH$_4$ is of similar origin in all five glacier forefields.

## 3.2 Spatial distribution of sediment-entrapped CH₄ contents in the GRF sampling zone

Methane contents in 52 samples collected from 20–70 cm depth ranged from 1.19 to 11.24 µg CH$_4$ g$^{-1}$ d.w., with one exceptionally high value at 40 cm depth (Fig. 5). Based on these data, there was no clear correlation between sediment depth and entrapped CH$_4$ contents (one-way ANOVA, $p = 0.9$). Thus, we subsequently proceeded to collect sediments from 20 cm depth only, and assumed these samples to be representative in terms of entrapped CH$_4$ content for the entire sediment thickness.

The effects of the proxies sediment age and landform on entrapped CH$_4$ contents were tested using sediments collected from 20 cm depth at 99 locations (Fig. 2a). The CH$_4$ contents in these samples ranged from 0.59 to 34.82 µg CH$_4$ g$^{-1}$ d.w. (Fig. 3b), with an average of 5.30 ($\pm$ 4.86) µg CH$_4$ g$^{-1}$ d.w.. Two-way ANOVA analysis indicated that landform had a significant effect on sediment-entrapped CH$_4$ contents ($p = 0.03$), whereas effects of sediment age ($p = 0.19$) and the combined effects of sediment age and landform on entrapped CH$_4$ contents ($p = 0.37$) were insignificant. Post-hoc comparisons using the Tukey HSD test indicated that mean values for sediment-entrapped CH$_4$ content (Table 1) were significantly different between floodplain and sandhill ($p = 0.03$), and weakly different between floodplain and terrace ($p = 0.10$). The difference between terrace and sandhill with respect to mean sediment-entrapped CH$_4$ content was insignificant ($p = 0.88$).

## 3.3 Mass of sediment-entrapped CH₄ in the GRF sampling zone

To estimate the mass of sediment-entrapped CH$_4$ stored within the GRF sampling zone, we used Eq. (1) with mean values on entrapped CH$_4$ contents, sediment thickness, and sediment-covered area determined for each of the three landforms (Table 1). Whereas $\overline{C}_{CH4}$ varied by a factor <1.4 between landforms, sediment thickness was highly variable along the five measured ERT profiles (range 1.0–31.5 m; Fig. 6, Fig. S3), and $\overline{T}_{sed}$ varied by a factor of ~2 between landforms (Table 1). Sediment-covered area also showed substantial variation between the different landforms. Within the GRF sampling zone, the sandhill landform comprised the largest sediment-covered area with $\overline{A}_{sed} \approx 10^5$ m$^2$, about 5 times larger than for floodplain and terrace. Consequently, the largest sediment mass was contained in the sandhill landform (factor 2–3 larger than floodplain and terrace, Table 1). All three landforms combined featured a surface area of ~1.5×10$^5$ m$^2$, and contained an estimated mass of ~2.4×10$^6$ t sediment. Adding up the masses of sediment-entrapped CH$_4$ for each landform yielded a total $\overline{m}_{CH4} = 9.7 \pm 3.0$ t CH$_4$. When calculated using average values for entrapped CH$_4$ contents and sediment thickness, and combined sediment-covered area, the estimated $\overline{m}_{CH4}$ within the GRF sampling zone was 12.7 $\pm$ 4.0 t CH$_4$ (last row in Table 1). Uncertainties in individual $\overline{m}_{CH4}$ values up to ~50% mostly arose from uncertainties in $\overline{T}_{sed}$ (dominated by the large variability in sediment thickness across the GRF sampling zone), and to a smaller degree from uncertainties in $\overline{C}_{CH4}$.

## 3.4 Contents and total mass of sediment-entrapped CH₄ in five glacier forefields

Methane contents varied substantially between different glacier forefields (Table 2), with distance between the forefields playing an apparently important role. Specifically, the IMG, GRF, and GRI glacier forefields are located in the Northeast of the Helvetic Nappes relatively close to each other (Fig. 1) and featured similar, low sediment-entrapped CH₄ contents. Likewise, the WIL and TSA glacier forefields are located close to each other in the Southwest of the Helvetic Nappes and featured similar, but high sediment-entrapped CH₄ contents. Indeed, our ANOVA results indicated that differences in sediment-entrapped CH₄ contents were insignificant between the IMG, GRF, and GRI glacier forefields ($p = 0.36$) and between the WIL and TSA glacier forefields ($p = 0.18$). Conversely, differences in entrapped CH₄ contents between the two groups of glacier forefields were highly significant ($p < 0.0001$).

The total mass of CH₄ entrapped in sediments of the five glacier forefields was calculated using estimated values for sediment thickness ($10.0 \pm 3.0$ m; the thickness measured in the GRF sampling zone (see above)) and sediment-particle density ($2.71 \pm 0.15$ g/cm³; Daly (1935)) that were assumed identical for all five forefields, as well as specific data for each glacier forefield on entrapped CH₄ contents, sediment-covered area, and sediment porosity (Table 2). Whereas $\overline{\theta}_{t,sed}$ values varied only little between the five forefields, $\overline{A}_{sed}$ varied up to a factor of ~3 (IMG vs. WIL), and $\overline{C}_{CH4}$ up to a factor of ~7 (GRF vs. WIL). This led to substantial differences in the estimated total mass of sediment-entrapped CH₄ between the five forefields, which ranged from $200 \pm 74$ t CH₄ for the GRF glacier forefield to $3881 \pm 1367$ t CH₄ for the WIL forefield (Fig. 7a). Estimates of sediment-entrapped CH₄ mass for the WIL and TSA glacier forefields were significantly larger than for IMG, GRF, and GRI. For all five forefields, sediment thickness and sediment-covered area contributed most to uncertainties in the quantification (Fig. 7b). Conversely, entrapped CH₄ contents, sediment porosity, and sediment-particle density together contributed $\leq 16\%$ to the calculated uncertainties.

## 3.5 Mass of sediment-entrapped CH₄ in all Swiss glacier forefields on calcareous bedrock

The first estimate of the total mass of sediment-entrapped CH₄ in all calcareous glacier forefields in Switzerland was based on published data on glacier retreat in the Swiss Alps, an estimation of the fraction of calcareous glacier-forefield surface area, mean values for sediment thickness, sediment-particle density and sediment porosity, as well as a mean value for sediment-entrapped CH₄ content obtained from the five investigated glacier forefields ($18.5 \pm 4.4$ µg CH₄ g⁻¹ d.w.; Table 3). Between the end of the Little Ice Age (~1850) and 2010, the glaciated area within the Swiss Alps has decreased by ~676 km² to less than 60 % of its original value (data sources see Table 3). When multiplied by the fraction of calcareous bedrock area in the Swiss Alps ($54.6 \pm 1.7$ %), this yielded an exposed calcareous glacier-forefield area of ~369 km². The total sediment mass contained within this exposed calcareous glacier-forefield area was then computed as $5.62 \times 10^9 \pm 1.46 \times 10^9$ t. From these numbers, we estimated the total mass of sediment-entrapped CH₄ in all Swiss glacier forefields derived from calcareous bedrock to $1.04 \times 10^5 \pm 3.7 \times 10^4$ t CH₄.

# 4 Discussion

## 4.1 Widespread occurrence of sediment-entrapped, thermogenic CH4 in calcareous glacier forefields

We detected substantial quantities of sediment-entrapped CH4 in all sampled glacier forefields. Entrapped CH4 was
330    ubiquitously encountered at different sediment depths, and in different forefield landforms and sediment-age classes. We also
detected entrapped CH4 in most bedrock samples obtained from these glacial catchments. Furthermore, our data indicated that
both sediment- and rock-entrapped CH4 are of thermogenic origin. Thus, the results presented here extend our previous studies
(Nauer et al., 2012; Zhu et al., 2018) by providing a more detailed survey on entrapped CH4 contained in glacier-forefield
sediments across the Helvetic Nappes, and support our hypothesis on its widespread occurrence and thermogenic origin in
335    calcareous, Swiss Alpine glacier forefields. On the other hand, we cannot entirely reject the possibility for the presence of
microbial CH4 sources in certain parts of glacier forefields, particularly in water-logged sediments. Methanogenic potential in
isolated hotspots of water-logged sediments was previously confirmed for the WIL glacier forefield, but considered to be of
minor importance under field conditions (Zhu et al., 2018). In the present study, no attempt was made to specifically identify
potential methanogenic hotspots in sediments of the other four glacier forefields.

340        Methane is commonly found in organic-rich sedimentary rocks such as shales, marls, and limestones as a product of
the thermal maturation of buried organic matter (Etiope, 2017; Horsfield and Rullkötter, 1994). Previous studies on fluid
inclusions in quartz and calcite minerals collected from Alpine fissures and veins within the Helvetic Nappes revealed the
existence of four fluid zones, including a large thermogenic CH4 zone (Gautschi et al., 1990; Mazurek et al., 1998; Mullis et
al., 1994; Tarantola et al., 2007). The five glacier forefields we sampled in this study were all located within or near the border
345    of this thermogenic CH4 zone (see Fig. 1 in Tarantola et al. (2007)). Our results thus agree with previous findings on the
occurrence of thermogenic CH4 in this region, including the occurrence of thermogenic CH4 detected in gas seeps near Giswil,
Central Switzerland, which lies on Penninic Flysch underlain by Helvetic Nappes (Etiope et al., 2010). On the other hand, our
results also show that CH4 entrapment within the Helvetic Nappes is not restricted to fluid inclusions in fissure minerals, but
that substantial quantities of CH4 are entrapped within the matrix of the sedimentary bedrock and sediment particles
350    themselves, presumably within inter- and intragranular micro- and macroporosity (Hashim and Kaczmarek, 2019; Moshier,
1989; Léonide et al., 2014; Abrams, 2017).

        Our geochemical data further indicate a common origin for CH4 entrapped in bedrock and glacier-forefield sediments,
derived from ancient terrestrial and marine organic matter (kerogen types III and II, respectively; Fig. 4). This provides further
evidence that CH4 entrapped in the forefield sediments of the Helvetic Nappes has its origin in the calcareous parent bedrock.
355    Moreover, terrestrial and marine organic matter as the ultimate source of sediment- and rock-entrapped CH4 agrees with the
origin of the Helvetic Nappes: their sediments and organic matter were originally deposited under highly variable climatic
conditions on the shallow northern shelf of the ancient Alpine Tethys Ocean (Weissert and Mohr, 1996; Weissert and Stössel,
2015).

## 4.2 Spatial distribution of sediment-entrapped CH$_4$ within and between glacier forefields

360  Sediment-entrapped CH$_4$ contents showed moderate variability within each glacier forefield (Fig. 3a-e). As sediments were largely derived by glacial erosion from the surrounding calcareous bedrock (Chesworth et al., 2008; Fu and Harbor, 2011), the observed variability in sediment-entrapped CH$_4$ contents reflects the variability in entrapped CH$_4$ contents of the various geological formations and associated mineralogy present in each catchment (Fig. 3f). Entrapped CH$_4$ contents in sedimentary bedrocks is typically affected by three main factors: the quantity and quality of organic matter buried during sediment

365  deposition, the thermal history during sediment diagenesis and subsequent organic matter catagenesis, and the resulting permeability of the calcareous bedrock, which affects potential gas migration (e.g., Dayal, 2017; Horsfield and Rullkötter, 1994; Mani et al., 2017). Whereas geological formations contained within the same nappe are expected to possess a similar thermal history, the quantity and quality of organic matter buried may vary substantially between individual formations depending on prevailing conditions during the period of sediment deposition (Weissert and Mohr, 1996; Weissert et al., 1985).

370  Thus, variability in rock- and sediment-entrapped CH$_4$ contents is to be expected for glacial catchments featuring geological formations from different time periods, as was observed for all of the glacier forefields sampled in this study (Table 2).

Our study in the GRF forefield sampling zone indicated that sediment-entrapped CH$_4$ content varied little with sediment depth (Fig. 5) and sediment age. However, we cannot exclude the possibility that such variations could be somewhat larger outside of the sampled depth interval, e.g., in top-layer sediments at depths < 5 cm as a result of enhanced chemical, physical,

375  or biological weathering (Bernasconi et al., 2011; van der Meij et al., 2016; Lazzaro et al., 2009). We refrained from collecting top-layer sediments because in all five glacier forefields they were generally much coarser and thus did not appear representative of bulk sediments present at greater depth. We assume that sediment fines are continuously removed from the top layer as a result of physical (wind and water) erosion.

On the other hand, we consider the lack of significant variation with sediment age as an indication that CH$_4$ in glacier-

380  forefield sediments is relatively stable in its entrapped state. This hypothesis is supported by results of our geochemical analyses for all five glacier forefields, which mostly indicated high similarity between sediment- and rock-entrapped CH$_4$ in terms of the range of measured CH$_4$ contents (Fig. 3f), as well as gas-wetness ratios and $\delta^{13}C_{CH4}$ values (Fig. 4). Thus, although sediments have undergone erosion from the parent bedrock and subsequent weathering, changes in entrapped CH$_4$ geochemical characteristics appeared negligible. This indicates that a potential release of entrapped CH$_4$ from sediment particles by

385  molecular diffusion, or oxidation of CH$_4$ in its entrapped state within sediment particles, may be small in magnitude, as these processes would be expected to cause a noticeable change in CH$_4$ geochemical characteristics (Schloemer and Krooss, 2004; Whiticar, 1999; Zhang and Krooss, 2001). Our findings therefore suggest that CH$_4$ entrapped in bedrock and sediment matrices resides largely in inaccessible, occluded rather than connected pore spaces. However, a potential release of entrapped CH$_4$ from occluded pore spaces may yet occur via sediment erosion processes, in particular by means of physical and/or chemical

390  weathering of calcareous minerals (Emmanuel and Levenson, 2014; Ryb et al., 2014; Trudgill and Viles, 1998). As these processes act on rock surfaces, they are of great important to sediments with large specific surface areas, the latter being

inversely related to particle size (Michel and Courard, 2014). Although we are aware that similar erosion processes will act upon large bedrock surfaces, e.g., rock walls and other outcrops within glacial catchments, we have so far refrained from considering $CH_4$ release from these locations because of the much smaller specific surface areas involved. Unfortunately, the release of entrapped $CH_4$ as a result of sediment erosion may not be detectable in the sediment's entrapped $CH_4$ contents, as both $CH_4$ and sediment mass is lost as a result of erosion. Hence, our present data set yields no information on the relevance of erosion processes for $CH_4$ release.

In contrast to sediment depth and sediment age, we detected a small but significant difference in mean sediment-entrapped $CH_4$ content between landforms within the GRF sampling zone. Specifically, mean entrapped $CH_4$ content in floodplain sediments was significantly higher than in terrace and sandhill sediments (Table 1). We can only speculate about possible reasons for this observation. One reason could be that floodplain sediments, intermittently removed and deposited by the glacial stream during and after flooding events, originate from locations outside of our sampling zone, i.e., from different parent bedrock (Fig. S2). It is therefore possible that we missed to sample parent bedrock types (e.g., from steep rock walls) with different (in this case higher) entrapped $CH_4$ contents in this or any of the other glacial catchments. An improved mineralogical investigation of sediments in the various landforms would aid in clarifying this issue.

Finally, our data revealed large regional differences in mean sediment-entrapped $CH_4$ contents between glacier forefields (Table 2). This may be explained by the fact that sediments in glacier forefields located in close proximity to one another are, at least in part, derived from the same individual nappes and geological formations contained therein. For example, both the WIL and TSA glacier forefields harbor sediments derived from the Wildhorn nappe, featuring several identical geological formations. Hence, this result supports our previous hypothesis that differences in lithology, mineralogy, and tectonic settings between individual nappes play an important role in determining bedrock- and thus sediment-entrapped $CH_4$ contents (Zhu et al., 2018). Regional differences in entrapped $CH_4$ contents paired with differences in sediment-covered area led to significant variation in the estimates for total mass of $CH_4$ stored in sediments of the five glacier forefields (Fig. 7a). Uncertainties associated with these estimates were reasonably small, and arose largely from uncertainties in sediment thickness and sediment-covered area (Fig. 7b). To further reduce these uncertainties, measurements of these parameters across entire glacier forefields would be of help using, e.g., geophysical methods for sediment thickness (such as the ERT method used in the GRF sampling zone), and field mapping of sediment-covered area in combination with GIS based methods utilizing digital elevation models (e.g., Geilhausen et al., 2012; Smith and Clark, 2005; Zemp et al., 2005). Unfortunately, field measurements in the rugged alpine environment are typically time-consuming, expensive, and challenging to perform.

### 4.3 A substantial quantity of sediment-entrapped $CH_4$ with yet unknown fate

Our first, rough estimate for the total quantity of $CH_4$ entrapped in sediments of all calcareous Swiss glacier forefields combined yielded a substantial mass of $1.04 \times 10^5 \pm 3.7 \times 10^4$ t $CH_4$, contained within a solid volume of ~2.1 km$^3$ glacier-forefield sediments. At first glance, this number appears large when compared with an estimate of annual $CH_4$ emissions to the atmosphere ($5.7 \times 10^3$ t $CH_4$) from natural and semi-natural sources in Switzerland, including emissions from lakes, reservoirs,

425 wetlands, and wild animals (Hiller et al., 2014). However, whereas the latter data represent annual $CH_4$ fluxes, the fate of sediment-entrapped $CH_4$ remains elusive to date (see below). On the other hand, our number is in good agreement with a previous estimate on $CH_4$ content for Valanginian marl, a geological formation within the Helvetic Nappes, containing calcite fracture fill ($\sim0.7\times10^5$–$2.1\times10^5$ t $CH_4$ km$^{-3}$ bedrock; Gautschi et al. (1990)).

Our estimate for total sediment-entrapped $CH_4$ mass is subject to substantial uncertainty. The two largest contributors
430 to the calculated uncertainty are sediment-entrapped $CH_4$ content and sediment thickness. In addition, there is considerable uncertainty in the exposed calcareous glacier-forefield area, as the latter was only roughly estimated based on glacier retreat and the fraction of calcareous bedrock area in the Swiss Alps. As discussed above for individual glacier forefields, field measurements and GIS based methods may help to reduce uncertainties related to sediment thickness and exposed area. An important way to reduce uncertainty related to entrapped $CH_4$ contents would be to generate a database of $CH_4$ contents for
435 different geological formations present within the Helvetic Nappes, as lithology and tectonic settings appear to control $CH_4$ contents. Determination of the areal extent of different geological formations would likely help to reduce uncertainties in sediment-entrapped $CH_4$ mass.

Whether or not sediment-entrapped $CH_4$ plays a role as an emission source to the atmosphere will largely depend upon its rate of release from sediment particles and its potential consumption by MOBs in aerated sediments. Whereas we produced
440 some evidence that $CH_4$ is stable in its entrapped state (see discussion above), further investigations will be required to specifically elucidate possible mechanisms and fluxes of $CH_4$ release in forefield sediments, in particular during periods of enhanced physical/chemical weathering, e.g., during rainstorms or snow melt (Winnick et al., 2017). Notably, atmospheric $CH_4$ oxidation was previously detected in several glacier forefields including our GRF site (Bárcena et al., 2011; Chiri et al., 2015; Hofmann et al., 2013). These studies indicated that MOB activity in forefield sediments establishes quickly (within the
445 first 10 years after glacier retreat), and fluxes of $CH_4$ uptake from the atmosphere increase to values comparable to mature soils within a few decades (Chiri et al., 2015). Nonetheless, intermittent $CH_4$ emissions to the atmosphere were also observed in GRF floodplain sediments (Chiri et al., 2017). Hence, we hypothesize that traces of $CH_4$ released from sediment particles may be consumed by MOB, at least under favorable environmental conditions, and serve as an additional source of energy and carbon to this group of microorganisms. This hypothesis, of course, awaits experimental confirmation.

450 **5 Summary and Conclusions**

Our results provide new evidence for the widespread occurrence of sediment-entrapped, thermogenic $CH_4$ in Swiss calcareous glacier forefields. As entrapped $CH_4$ with highly similar geochemical characteristics was also detected in most bedrock samples collected from nearby geological formations, we conclude that $CH_4$ entrapped in forefield sediments of the Helvetic Nappes has its origin in the calcareous parent bedrock. Hence, spatial variability in sediment-entrapped $CH_4$ contents within glacier
455 forefields largely reflects the variability in entrapped $CH_4$ contents of the surrounding bedrock types.

Within glacier forefields, sediment-entrapped $CH_4$ contents and other geochemical characteristics showed little systematic variation with sediment age and thus time of exposure to the atmosphere following glacier retreat. Together with the noted similarity in geochemical characteristics we took this finding as evidence that $CH_4$ in glacier-forefield sediments is relatively stable in its entrapped state, presumably because it resides in occluded pore spaces within bedrock and sediment matrices. This further indicates that $CH_4$ entrapment within the Helvetic Nappes is not restricted to fluid inclusions in fissure minerals, but that substantial quantities of $CH_4$ are entrapped within the matrix of the sedimentary bedrock and sediment particles themselves. On the other hand, our results revealed large regional differences in mean sediment-entrapped $CH_4$ contents between glacier forefields, supporting our previous hypothesis that differences in lithology and tectonic settings between individual nappes play an important role in determining bedrock- and thus sediment-entrapped $CH_4$ contents.

*Data availability*. The data used in this manuscript will be made available on ETH Zurich Research Collection after the manuscript is published.

*Supplement*. The supplement related to this article is available online at: …..

*Author contribution*. BZ, MR, MK, and MHS helped with sample collection and/or geochemical measurements, and substantially contributed to the interpretation of data. DB helped with ERT measurements and subsequent ERT data analyses. BZ and MHS wrote the manuscript. MHS designed the study and acquired the funding for the project. All authors commented on the manuscript and approved the final version of the manuscript.

*Competing interests*. The authors declare that they have no conflict of interest.

*Acknowledgements*. We are grateful to S. Bernasconi (ETHZ) and C. Schubert (EAWAG) for assistance with stable isotope analyses, and to S. Bernasconi for providing valuable suggestions to an early version of this manuscript. We thank L. Baron (UNIL) for introducing us to initial ERT measurements in glacial systems, and P. Erickson, M. Meola, and S. Meyer (all ETHZ) for their help during ERT field campaigns. We also thank C., F., and M. Stadler (Altdorf, UR) for granting road access to the GRF site. We acknowledge D. Archer and an anonymous Referee for providing valuable comments and suggestions to our manuscript.

*Financial support*. This research project was funded by the Swiss National Science Foundation under grant no. 200021_153571. Additional funding was received from ETH Zurich.

*Review statement*. This paper was edited by T. Treude and reviewed by D. Archer and an anonymous referee.

## References

Abrams, M. A.: Evaluation of Near-Surface Gases in Marine Sediments to Assess Subsurface Petroleum Gas Generation and Entrapment, Geosciences, 7, 10.3390/geosciences7020035, 2017.

André, M., Malmstrom, M. E., and Neretnieks, I.: Specific surface area determinations on intact drillcores and evaluation of extrapolation methods for rock matrix surfaces, J Contam Hydrol, 110, 1-8, 10.1016/j.jconhyd.2009.05.003, 2009.

Bárcena, T. G., Yde, J. C., and Finster, K. W.: Methane flux and high-affinity methanotrophic diversity along the chronosequence of a receding glacier in Greenland, Ann Glaciol, 51, 23-31, 2010.

Bárcena, T. G., Finster, K. W., and Yde, J. C.: Spatial Patterns of Soil Development, Methane Oxidation, and Methanotrophic Diversity along a Receding Glacier Forefield, Southeast Greenland, Arct Antarct Alp Res, 43, 178-188, 10.1657/1938-4246-43.2.178, 2011.

Bastviken, D., Tranvik, L. J., Downing, J. A., Crill, P. M., and Enrich-Prast, A.: Freshwater methane emissions offset the continental carbon sink, Science, 331, 50-50, 2011.

Bernard, B. B., Brooks, J. M., and Sackett, W. M.: Light-Hydrocarbons in Recent Texas Continental-Shelf and Slope Sediments, J Geophys Res-Oceans, 83, 4053-4061, 10.1029/JC083iC08p04053, 1978.

Bernasconi, S. M., Bauder, A., Bourdon, B., Brunner, I., Bunemann, E., Christl, I., Derungs, N., Edwards, P., Farinotti, D., Frey, B., Frossard, E., Furrer, G., Gierga, M., Goransson, H., Gulland, K., Hagedorn, F., Hajdas, I., Hindshaw, R., Ivy-Ochs, S., Jansa, J., Jonas, T., Kiczka, M., Kretzschmar, R., Lemarchand, E., Luster, J., Magnusson, J., Mitchell, E. A. D., Venterink, H. O., Plotze, M., Reynolds, B., Smittenberg, R. H., Stahli, M., Tamburini, F., Tipper, E. T., Wacker, L., Welc, M., Wiederhold, J. G., Zeyer, J., Zimmermann, S., and Zumsteg, A.: Chemical and Biological Gradients along the Damma Glacier Soil Chronosequence, Switzerland, Vadose Zone J., 10, 867-883, 10.2136/vzj2010.0129, 2011.

Bousquet, P., Ciais, P., Miller, J. B., Dlugokencky, E. J., Hauglustaine, D. A., Prigent, C., Van der Werf, G. R., Peylin, P., Brunke, E. G., Carouge, C., Langenfelds, R. L., Lathiere, J., Papa, F., Ramonet, M., Schmidt, M., Steele, L. P., Tyler, S. C., and White, J.: Contribution of anthropogenic and natural sources to atmospheric methane variability, Nature, 443, 439-443, 10.1038/nature05132, 2006.

Burns, R., Wynn, P. M., Barker, P., McNamara, N., Oakley, S., Ostle, N., Stott, A. W., Tuffen, H., Zhou, Z., Tweed, F. S., Chesler, A., and Stuart, M.: Direct isotopic evidence of biogenic methane production and efflux from beneath a temperate glacier, Sci Rep, 8, 10.1038/s41598-018-35253-2, 2018.

Chesworth, W., Perez-Alberti, A., and Arnaud, E.: Ice Erosion, in: Encyclopedia of Soil Science, edited by: Chesworth, W., Springer Netherlands, Dordrecht, 333-338, 2008.

Chiri, E., Nauer, P. A., Henneberger, R., Zeyer, J., and Schroth, M. H.: Soil-methane sink increases with soil age in forefields of Alpine glaciers, Soil Biol Biochem, 84, 83-95, 10.1016/j.soilbio.2015.02.003, 2015.

Chiri, E., Nauer, P. A., Rainer, E.-M., Zeyer, J., and Schroth, M. H.: High Temporal and Spatial Variability of Atmospheric-Methane Oxidation in Alpine Glacier Forefield Soils, Appl Environ Microb, 83, e01139-01117, 2017.

Christiansen, J. R., and Jørgensen, C. J.: First observation of direct methane emission to the atmosphere from the subglacial domain of the Greenland Ice Sheet, Sci Rep, 8, 16623, 10.1038/s41598-018-35054-7, 2018.

Christner, B. C., Montross, G. G., and Priscu, J. C.: Dissolved gases in frozen basal water from the NGRIP borehole: implications for biogeochemical processes beneath the Greenland Ice Sheet, Polar Biol, 35, 1735-1741, 10.1007/s00300-012-1198-z, 2012.

Ciais, P., Sabine, C., Bala, G., Bopp, L., Brovkin, V., Canadell, J., Chhabra, A., DeFries, R., Galloway, J., Heimann, M., Jones, C., Quéré, C. L., Myneni, R. B., Piao, S., and Thornton, P.: Carbon and Other Biogeochemical Cycles, Cambridge University Press, United Kingdom and New York, NY, USA, 2013.

Conrad, R.: Soil microorganisms as controllers of atmospheric trace gases (H2, CO, CH4, OCS, N2O, and NO), Microbiol Rev, 60, 609-640, 1996.

Conrad, R.: The global methane cycle: recent advances in understanding the microbial processes involved, Env Microbiol Rep, 1, 285-292, 2009.

Curry, C. L.: The consumption of atmospheric methane by soil in a simulated future climate, Biogeosciences, 6, 2355-2367, 10.5194/bg-6-2355-2009, 2009.

Daly, R. A.: Densities of rocks calculated from their chemical analyses, P Natl Acad Sci USA, 21, 657-663, 10.1073/pnas.21.12.657, 1935.

Dayal, A. M.: Chapter 2 - Deposition and Diagenesis, in: Shale Gas, edited by: Dayal, A. M., and Mani, D., Elsevier, Amsterdam, NL, 13-23, 2017.

Denman, K. L., Brasseur, G. P., Chidthaisong, A., Ciais, P., Cox, P. M., Dickinson, R. E., Hauglustaine, D. A., Heinze, C., Holland, E. A., and Jacob, D. J.: Couplings between changes in the climate system and biogeochemistry, in: Climate change 2007: The physical science basis, Cambridge University Press, 2007.

Dlugokencky, E. J.: Trends in Atmospheric Methane: www.esrl.noaa.gov/gmd/ccgg/trends_ch4/, access: May 17, 2018, 2018.

Dunfield, P. F.: The Soil Methane Sink, in: Greenhouse Gas Sinks, edited by: Reay, D., Hewitt, C. N., Smith, K. A., and Grace, J., CABI, Wallingford, UK, 152-170, 2007.

Emmanuel, S., and Levenson, Y.: Limestone weathering rates accelerated by micron-scale grain detachment, Geology, 42, 751-754, 10.1130/G35815.1, 2014.

545    Etiope, G., Lassey, K. R., Klusman, R. W., and Boschi, E.: Reappraisal of the fossil methane budget and related emission from geologic sources, Geophys Res Lett, 35, L09307, 10.1029/2008GL033623, 2008.

Etiope, G., Zwahlen, C., Anselmetti, F. S., Kipfer, R., and Schubert, C. J.: Origin and flux of a gas seep in the Northern Alps (Giswil, Switzerland), Geofluids, 10, 476-485, 10.1111/j.1468-8123.2010.00302.x, 2010.

Etiope, G.: Climate science: Methane uncovered, Nature Geosci, 5, 373-374, 10.1038/ngeo1483, 2012.

550    Etiope, G., and Sherwood Lollar, B.: Abiotic methane on earth, Rev Geophys, 51, 276-299, 10.1002/rog.20011, 2013.

Etiope, G., and Schoell, M.: Abiotic Gas: Atypical, But Not Rare, Elements, 10, 291-296, 10.2113/gselements.10.4.291, 2014.

Etiope, G.: Natural Gas, in: Encyclopedia of Geochemistry: A Comprehensive Reference Source on the Chemistry of the Earth, edited by: White, W. M., Springer International Publishing, Cham, 1-5, 2017.

Etiope, G., Ifandi, E., Nazzari, M., Procesi, M., Tsikouras, B., Ventura, G., Steele, A., Tardini, R., and Szatmari, P.: Widespread abiotic
555    methane in chromitites, Sci Rep, 8, 8728, 10.1038/s41598-018-27082-0, 2018.

Fischer, M., Huss, M., Barboux, C., and Hoelzle, M.: The new Swiss Glacier Inventory SGI2010: relevance of using high-resolution source data in areas dominated by very small glaciers, Arct Antarct Alp Res, 46, 933-945, 10.1657/1938-4246-46.4.933, 2014.

Fu, P., and Harbor, J.: Glacial Erosion, in: Encyclopedia of Snow, Ice and Glaciers, edited by: Singh, V. P., Singh, P., and Haritashya, U. K., Springer Netherlands, Dordrecht, 332-341, 2011.

560    Gautschi, A., Faber, E., Meyer, J., Mullis, J., Schenker, F., and Ballentine, C.: Hydrocarbon and noble gases in fluid inclusions of alpine calcite veins: implications for hydrocarbon exploration, Bulletin der Vereinigung Schweizerischer Petroleum-Geologen und-Ingenieure, 57, 13-36, 1990.

Geilhausen, M., Otto, J. C., and Schrott, L.: Spatial distribution of sediment storage types in two glacier landsystems (Pasterze & Obersulzbachkees, Hohe Tauern, Austria), J Maps, 8, 242-259, 10.1080/17445647.2012.708540, 2012.

565    Haeberli, W., Hoelzle, M., Paul, F., and Zemp, M.: Integrated monitoring of mountain glaciers as key indicators of global climate change: the European Alps, Ann Glaciol, 46, 150-160, 10.3189/172756407782871512, 2007.

Hashim, M. S., and Kaczmarek, S. E.: A review of the nature and origin of limestone microporosity, Mar Petrol Geol, 107, 527-554, 10.1016/j.marpetgeo.2019.03.037, 2019.

Herwegh, M., and Pfiffner, O. A.: Tectono-metamorphic evolution of a nappe stack: A case study of the Swiss Alps, Tectonophysics, 404,
570    55-76, 10.1016/j.tecto.2005.05.002, 2005.

Hiller, R., Bretscher, D., DelSontro, T., Diem, T., Eugster, W., Henneberger, R., Hobi, S., Hodson, E., Imer, D., and Kreuzer, M.: Anthropogenic and natural methane fluxes in Switzerland synthesized within a spatially explicit inventory, Biogeosciences, 11, 1941-1959, 2014.

Hofmann, K., Reitschuler, C., and Illmer, P.: Aerobic and anaerobic microbial activities in the foreland of a receding glacier, Soil Biol
575    Biochem, 57, 418-426, 10.1016/j.soilbio.2012.08.019, 2013.

Horsfield, B., and Rullkötter, J.: Diagenesis,Catagenesis, and Metagenesis of Organic Matter, in: The Petroleum System—From Source to Trap, edited by: Magoon, L. B., and Dow, W. G., AAPG Memoir, Tulsa, OK, USA, 189-200, 1994.

Jackson, R. E., Gorody, A. W., Mayer, B., Roy, J. W., Ryan, M. C., and Van Stempvoort, D. R.: Groundwater protection and unconventional gas extraction: the critical need for field-based hydrogeological research, Ground Water, 51, 488-510, 10.1111/gwat.12074, 2013.

580    Joye, S. B.: A piece of the methane puzzle, Nature, 491, 538, 10.1038/nature11749, 2012.

Kirschke, S., Bousquet, P., Ciais, P., Saunois, M., Canadell, J. G., Dlugokencky, E. J., Bergamaschi, P., Bergmann, D., Blake, D. R., Bruhwiler, L., Cameron-Smith, P., Castaldi, S., Chevallier, F., Feng, L., Fraser, A., Heimann, M., Hodson, E. L., Houweling, S., Josse, B., Fraser, P. J., Krummel, P. B., Lamarque, J.-F., Langenfelds, R. L., Le Quere, C., Naik, V., O'Doherty, S., Palmer, P. I., Pison, I., Plummer, D., Poulter, B., Prinn, R. G., Rigby, M., Ringeval, B., Santini, M., Schmidt, M., Shindell, D. T., Simpson, I. J., Spahni, R.,
585    Steele, L. P., Strode, S. A., Sudo, K., Szopa, S., van der Werf, G. R., Voulgarakis, A., van Weele, M., Weiss, R. F., Williams, J. E., and Zeng, G.: Three decades of global methane sources and sinks, Nature Geosci, 6, 813-823, 10.1038/ngeo1955, 2013.

Kneisel, C.: Assessment of subsurface lithology in mountain environments using 2D resistivity imaging, Geomorphology, 80, 32-44, 10.1016/j.geomorph.2005.09.012, 2006.

Kneisel, C., and Kääb, A.: Mountain permafrost dynamics within a recently exposed glacier forefield inferred by a combined
590    geomorphological, geophysical and photogrammetrical approach, Earth Surf Proc Land, 32, 1797-1810, 10.1002/esp.1488, 2007.

Lamarche-Gagnon, G., Wadham, J. L., Lollar, B. S., Arndt, S., Fietzek, P., Beaton, A. D., Tedstone, A. J., Telling, J., Bagshaw, E. A., and Hawkings, J. R.: Greenland melt drives continuous export of methane from the ice-sheet bed, Nature, 565, 73, 10.1038/s41586-018-0800-0, 2019.

Lazzaro, A., Abegg, C., and Zeyer, J.: Bacterial community structure of glacier forefields on siliceous and calcareous bedrock, Eur J Soil
595    Sci, 60, 860-870, 10.1111/j.1365-2389.2009.01182.x, 2009.

Léonide, P., Fournier, F., Reijmer, J. J. G., Vonhof, H., Borgomano, J., Dijk, J., Rosenthal, M., van Goethem, M., Cochard, J., and Meulenaars, K.: Diagenetic patterns and pore space distribution along a platform to outer-shelf transect (Urgonian limestone, Barremian-Aptian, SE France), Sediment Geol, 306, 1-23, 10.1016/j.sedgeo.2014.03.001, 2014.

Loke, M.: Tutorial: 2-D and 3-D Electrical Imaging Surveys, Course Notes for USGS Workshop "2-D and 3-D Inversion and Modeling of
600    Surface and Borehole Resistivity Data", Storrs, CT, USA, March 13-16, 2001, 2001.

Loke, M. H., and Barker, R. D.: Rapid least-squares inversion of apparent resistivity pseudosections by a quasi-Newton method, Geophys Prospect, 44, 131-152, 10.1111/j.1365-2478.1996.tb00142.x, 1996.

Mani, D., Kalpana, M. S., Patil, D. J., and Dayal, A. M.: Chapter 3 - Organic Matter in Gas Shales: Origin, Evolution, and Characterization, in: Shale Gas, edited by: Dayal, A. M., and Mani, D., Elsevier, Amsterdam, NL, 25-54, 2017.

605 Martini, A. M., Walter, L. M., Ku, T. C., Budai, J. M., McIntosh, J. C., and Schoell, M.: Microbial production and modification of gases in sedimentary basins: A geochemical case study from a Devonian shale gas play, Michigan basin, AAPG Bull, 87, 1355-1375, 10.1306/031903200184, 2003.

Mazurek, M., Water, H., and Gautschi, A.: Hydrocarbon gases and fluid evolution in very low-grade metamorphic terranes: A case study from the Central Swiss Alps, in: Water-Rock Interaction, edited by: Arehart, G. B., and Hulston, J. R., Balkema, Rotterdam, NL, 417-

610 420, 1998.

Michel, F., and Courard, L.: Particle Size Distribution of Limestone Fillers: Granulometry and Specific Surface Area Investigations, Particul Sci Technol, 32, 334-340, 10.1080/02726351.2013.873503, 2014.

Milkov, A. V., and Etiope, G.: Revised genetic diagrams for natural gases based on a global dataset of > 20,000 samples, Org Geochem, 125, 109-120, 10.1016/j.orggeochem.2018.09.002, 2018.

615 Moshier, S. O.: Microporosity in Micritic Limestones - a Review, Sediment Geol, 63, 191-213, 10.1016/0037-0738(89)90132-2, 1989.

Mullis, J., Dubessy, J., Poty, B., and Oneil, J.: Fluid Regimes during Late Stages of a Continental Collision - Physical, Chemical, and Stable-Isotope Measurements of Fluid Inclusions in Fissure Quartz from a Geotraverse through the Central Alps, Switzerland, Geochim Cosmochim Ac, 58, 2239-2267, 10.1016/0016-7037(94)90008-6, 1994.

Nauer, P. A., Dam, B., Liesack, W., Zeyer, J., and Schroth, M. H.: Activity and diversity of methane-oxidizing bacteria in glacier forefields

620 on siliceous and calcareous bedrock, Biogeosciences, 9, 2259-2274, 10.5194/bg-9-2259-2012, 2012.

Nauer, P. A., Chiri, E., Zeyer, J., and Schroth, M. H.: Technical Note: Disturbance of soil structure can lead to release of entrapped methane in glacier forefield soils, Biogeosciences, 11, 613-620, 10.5194/bg-11-613-2014, 2014.

Paul, F., Kääb, A., Maisch, M., Kellenberger, T., and Haeberli, W.: Rapid disintegration of Alpine glaciers observed with satellite data, Geophys Res Lett, 31, L21402, 10.1029/2004GL020816, 2004.

625 Pfiffner, O. A.: Geology of the Alps, 2nd ed., Wiley Blackwell, Chichester, West Sussex, UK, 376 pp., 2014.

Reynolds, J. M.: An Introduction to Applied and Environmental Geophysics, John Wiley & Sons, Chichester, England, 1997.

Rowe, D., and Muehlenbachs, A.: Low-temperature thermal generation of hydrocarbon gases in shallow shales, Nature, 398, 61-63, 10.1038/18007, 1999.

Ryb, U., Matmon, A., Erel, Y., Haviv, I., Katz, A., Starinsky, A., Angert, A., and Team, A.: Controls on denudation rates in tectonically

630 stable Mediterranean carbonate terrain, Geol Soc Am Bull, 126, 553-568, 10.1130/B30886.1, 2014.

Saunois, M., Bousquet, P., Poulter, B., Peregon, A., Ciais, P., Canadell, J. G., Dlugokencky, E. J., Etiope, G., Bastviken, D., Houweling, S., Janssens-Maenhout, G., Tubiello, F. N., Castaldi, S., Jackson, R. B., Alexe, M., Arora, V. K., Beerling, D. J., Bergamaschi, P., Blake, D. R., Brailsford, G., Brovkin, V., Bruhwiler, L., Crevoisier, C., Crill, P., Covey, K., Curry, C., Frankenberg, C., Gedney, N., Höglund-Isaksson, L., Ishizawa, M., Ito, A., Joos, F., Kim, H. S., Kleinen, T., Krummel, P., Lamarque, J. F., Langenfelds, R., Locatelli, R.,

635 Machida, T., Maksyutov, S., McDonald, K. C., Marshall, J., Melton, J. R., Morino, I., Naik, V., O'Doherty, S., Parmentier, F. J. W., Patra, P. K., Peng, C., Peng, S., Peters, G. P., Pison, I., Prigent, C., Prinn, R., Ramonet, M., Riley, W. J., Saito, M., Santini, M., Schroeder, R., Simpson, I. J., Spahni, R., Steele, P., Takizawa, A., Thornton, B. F., Tian, H., Tohjima, Y., Viovy, N., Voulgarakis, A., van Weele, M., van der Werf, G. R., Weiss, R., Wiedinmyer, C., Wilton, D. J., Wiltshire, A., Worthy, D., Wunch, D., Xu, X., Yoshida, Y., Zhang, B., Zhang, Z., and Zhu, Q.: The global methane budget 2000–2012, Earth Syst Sci Data, 8, 697-751, 10.5194/essd-8-697-

640 2016, 2016.

Scapozza, C., Lambiel, C., Baron, L., Marescot, L., and Reynard, E.: Internal structure and permafrost distribution in two alpine periglacial talus slopes, Valais, Swiss Alps, Geomorphology, 132, 208-221, 10.1016/j.geomorph.2011.05.010, 2011.

Schloemer, S., and Krooss, B. M.: Molecular transport of methane, ethane and nitrogen and the influence of diffusion on the chemical and isotopic composition of natural gas accumulations, Geofluids, 4, 81-108, 10.1111/j.1468-8123.2004.00076.x, 2004.

645 Schoell, M.: Multiple origins of methane in the Earth, Chem Geol, 71, 1-10, 10.1016/0009-2541(88)90101-5, 1988.

Smith, M. J., and Clark, C. D.: Methods for the visualization of digital elevation models for landform mapping, Earth Surf Proc Land, 30, 885-900, 10.1002/esp.1210, 2005.

Souchez, R., Lemmens, M., and Chappellaz, J.: Flow-induced mixing in the GRIP basal ice deduced from the CO2 and CH4 records, Geophys Res Lett, 22, 41-44, 10.1029/94GL02863, 1995.

650 Stibal, M., Wadham, J. L., Lis, G. P., Telling, J., Pancost, R. D., Dubnick, A., Sharp, M. J., Lawson, E. C., Butler, C. E. H., Hasan, F., Tranter, M., and Anesio, A. M.: Methanogenic potential of Arctic and Antarctic subglacial environments with contrasting organic carbon sources, Glob Change Biol, 18, 3332-3345, 10.1111/j.1365-2486.2012.02763.x, 2012.

Tarantola, A., Mullis, J., Vennemann, T., Dubessy, J., and de Capitani, C.: Oxidation of methane at the CH4/H2O–(CO2) transition zone in the external part of the Central Alps, Switzerland: Evidence from stable isotope investigations, Chem Geol, 237, 329-357,

655 10.1016/j.chemgeo.2006.07.007, 2007.

Trudgill, S. T., and Viles, H. A.: Field and laboratory approaches to limestone weathering, Q J Eng Geol Hydroge, 31, 333-341, Doi 10.1144/Gsl.Qjeg.1998.031.P4.06, 1998.

UNEP, and WGMS: Global glacier changes: facts and figures, United Nations Environment Programme and World Glacier Monitoring Service, Geneva, Switzerland, 88 pp., 2008.

660  van der Meij, W. M., Temme, A. J. A. M., de Kleijn, C. M. F. J. J., Reimann, T., Heuvelink, G. B. M., Zwoliński, Z., Rachlewicz, G., Rymer, K., and Sommer, M.: Arctic soil development on a series of marine terraces on central Spitsbergen, Svalbard: a combined geochronology, fieldwork and modelling approach, SOIL, 2, 221-240, 10.5194/soil-2-221-2016, 2016.

Wadham, J. L., Arndt, S., Tulaczyk, S., Stibal, M., Tranter, M., Telling, J., Lis, G. P., Lawson, E., Ridgwell, A., Dubnick, A., Sharp, M. J., Anesio, A. M., and Butler, C. E. H.: Potential methane reservoirs beneath Antarctica, Nature, 488, 633-637, 10.1038/nature11374,
665  2012.

Wadham, J. L., De'ath, R., Monteiro, F. M., Tranter, M., Ridgwell, A., Raiswell, R., and Tulaczyk, S.: The potential role of the Antarctic Ice Sheet in global biogeochemical cycles, Earth Env Sci T R So, 104, 55-67, 10.1017/s1755691013000108, 2013.

Weissert, H., and Mohr, H.: Late Jurassic climate and its impact on carbon cycling, Palaeogeogr Palaeocl, 122, 27-43, 10.1016/0031-0182(95)00088-7, 1996.

670  Weissert, H., and Stössel, I.: Der Ozean im Gebirge - Eine geologische Zeitreise durch die Schweiz (in German), 3rd ed., vdf Hochschulverlag AG, ETH Zurich, Zurich, Switzerland, 2015.

Weissert, H. J., McKenzie, J. A., and Channell, J. E. T.: Natural Variations in the Carbon Cycle During the Early Cretaceous, The Carbon Cycle and Atmospheric CO2: Natural Variations Archean to Present, 32, 531-545, 10.1029/GM032p0531, 1985.

Whiticar, M. J.: Carbon and hydrogen isotope systematics of bacterial formation and oxidation of methane, Chem Geol, 161, 291-314,
675  10.1016/S0009-2541(99)00092-3, 1999.

Winnick, M. J., Carroll, R. W. H., Williams, K. H., Maxwell, R. M., Dong, W. M., and Maher, K.: Snowmelt controls on concentration-discharge relationships and the balance of oxidative and acid-base weathering fluxes in an alpine catchment, East River, Colorado, Water Resour Res, 53, 2507-2523, 10.1002/2016wr019724, 2017.

Zemp, M., Kaab, A., Hoelzle, M., and Haeberli, W.: GIS-based modelling of glacial sediment balance, Z Geomorphol Supp, 138, 113-129,
680  10.5167/uzh-40580, 2005.

Zemp, M., Paul, F., Hoelzle, M., and Haeberli, W.: Glacier Fluctuations in the European Alps, 1850–2000, in: Darkening Peaks - Glacier Retreat, Science, and Society, edited by: Orlove, B., Wiegandt, E., and Luckman, B. H., University of California Press, Oakland, CA, USA, 296, 2008.

Zhang, T. W., and Krooss, B. M.: Experimental investigation on the carbon isotope fractionation of methane during gas migration by
685  diffusion through sedimentary rocks at elevated temperature and pressure, Geochim Cosmochim Ac, 65, 2723-2742, 10.1016/S0016-7037(01)00601-9, 2001.

Zhu, B., Henneberger, R., Weissert, H., Zeyer, J., and Schroth, M. H.: Occurrence and Origin of Methane Entrapped in Sediments and Rocks of a Calcareous, Alpine Glacial Catchment, J Goephys Res-Biogeo, 123, 3633-3648, 10.1029/2018JG004651, 2018.

Zhuang, Q., Chen, M., Xu, K., Tang, J., Saikawa, E., Lu, Y., Melillo, J. M., Prinn, R. G., and McGuire, A. D.: Response of global soil
690  consumption of atmospheric methane to changes in atmospheric climate and nitrogen deposition, Global Biogeochem Cy, 27, 650-663, 10.1002/gbc.20057, 2013.

**Figures**
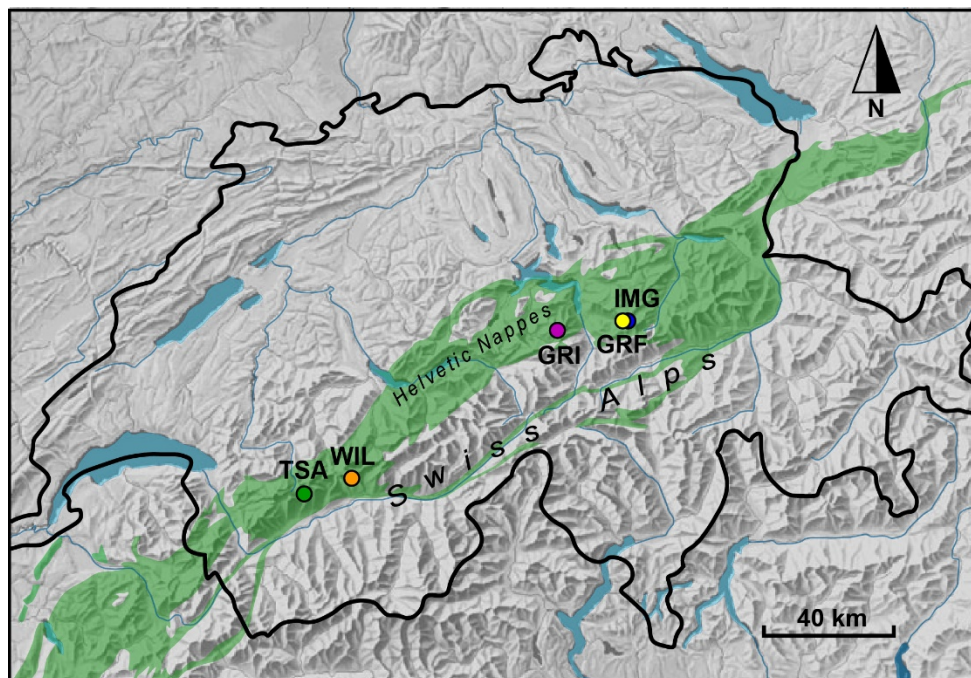
695

**Figure 1.** Map of Switzerland showing five glacier forefields from which sediment and bedrock samples were collected (Central Switzerland: Im Griess, IMG; Griessfirn, GRF; Griessen, GRI; Canton Valais: Wildstrubel, WIL; Tsanfleuron, TSA). All forefields are located within the Helvetic Nappes (green-shaded area), which consist largely of Mesozoic limestones, shales, and marls (map modified from Weissert and Stössel (2015)).

700
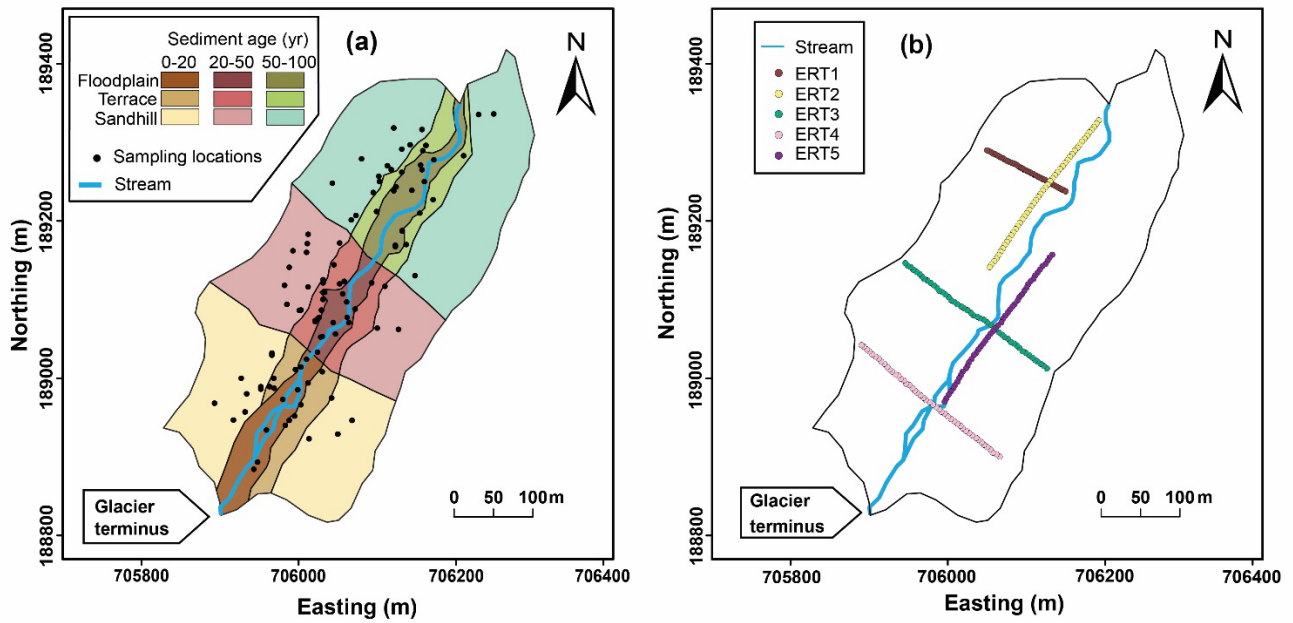
**Figure 2.** Sampling zone at Griessfirn (GRF) glacier forefield showing (a) blocks and sampling locations to study the effect of sediment age and glacier-forefield landforms (used here as proxies for all edaphic variations present in these sediments) on entrapped $CH_4$ contents, and (b) locations of five electrical resistivity tomography (ERT) profiles to measure sediment thickness. Axes show the Swiss CH1903/LV03 coordinate system (units in meters).
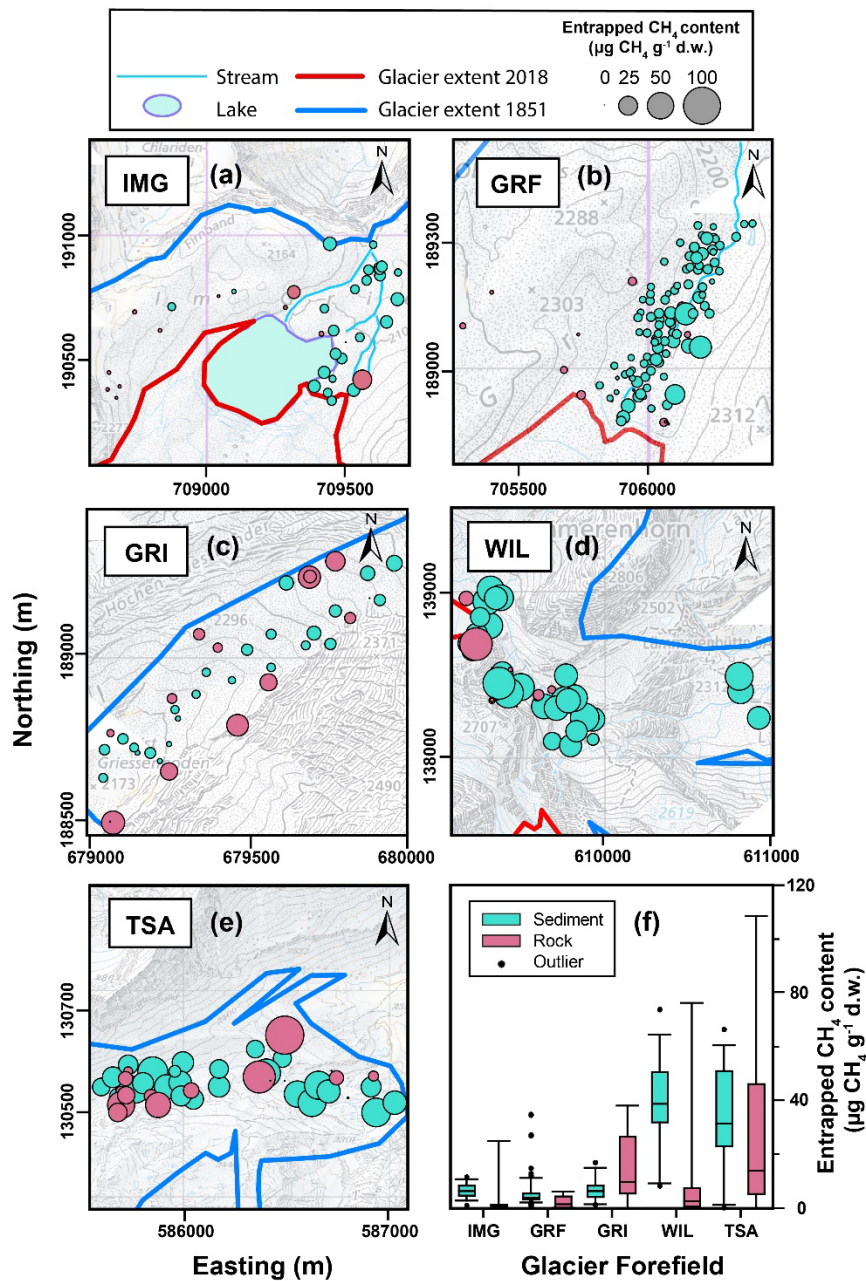
**Figure 3.** Spatial distribution of entrapped CH4 contents in sediments (blue bubbles) and rocks (red bubbles) collected from (a) Im Griess (IMG), (b) Griessfirn (GRF), (c) Griessen (GRI), (d) Wildstrubel (WIL), and (e) Tsanfleuron (TSA) glacier forefields (bubble size proportional to entrapped CH4 content). Background elevation data modified from swisstopo (Swiss Federal Office of Topography; maps.geo.admin.ch); axes show the Swiss CH1903/LV03 coordinate system (units in meters). (f) Box-whisker plot showing the range of entrapped CH4 contents in sediments and rocks for each glacier forefield. Boxes represent 25th, 50th (median), and 75th percentile; whiskers indicate 5th and 95th percentile, outliers are marked as dots.
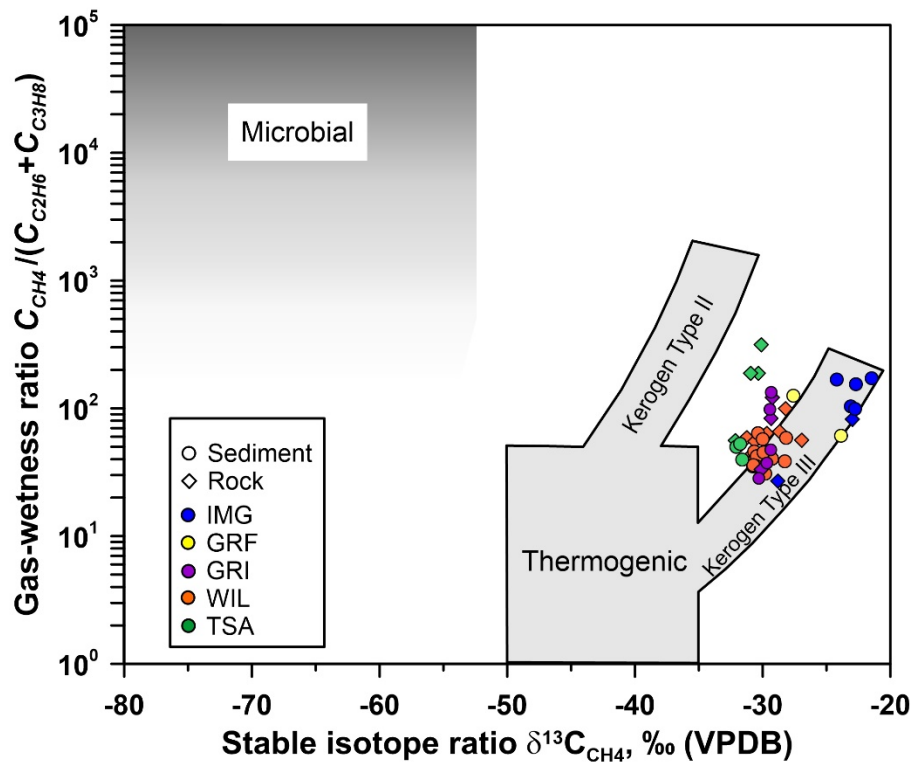
**Figure 4.** Adapted Bernard diagram (Bernard et al., 1978) showing gas-wetness ratio ($C_{CH4} / (C_{C2H6} + C_{C3H8})$) versus $\delta^{13}C_{CH4}$ for gas released from selected sediment and rock samples collected from Im Griess (IMG), Griessfirn (GRF), Griessen (GRI), Wildstrubel (WIL), and Tsanfleuron (TSA) glacier forefields. Grey-shaded areas indicate different $CH_4$ origins (microbial vs. thermogenic).

720
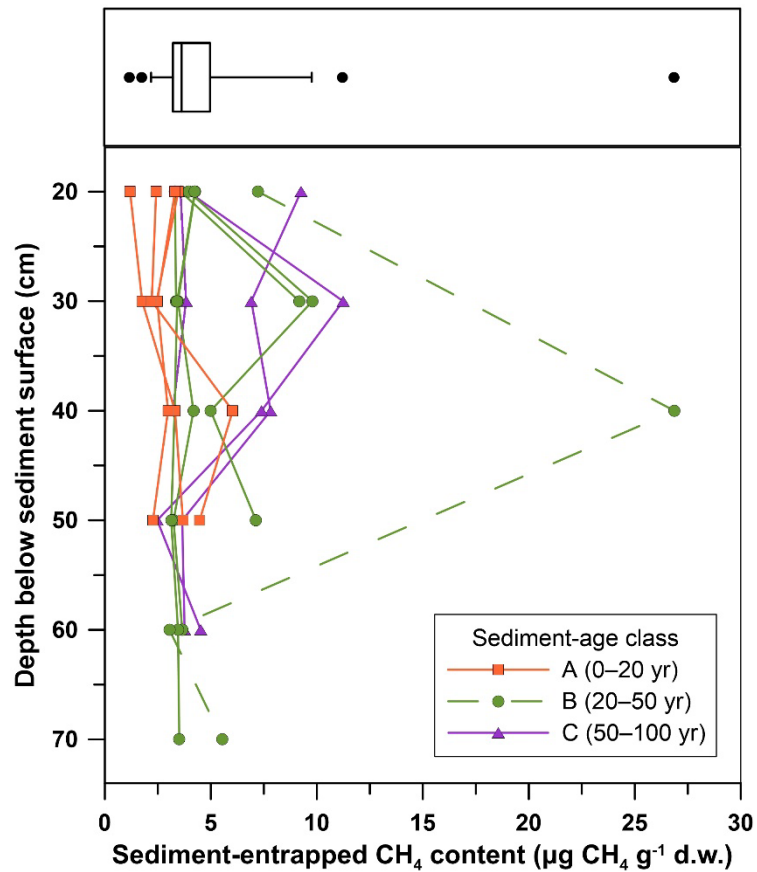
**Figure 5.** Sediment-entrapped CH₄ contents as a function of sediment depth for samples collected in three sediment-age classes in the Griessfirn (GRF) sampling zone. The box-whisker plot on top shows the range of entrapped CH₄ contents displayed below, with the box representing 25th, 50th (median), and 75th percentile; whiskers indicate the 5th and 95th percentile, outliers are marked as dots.

725
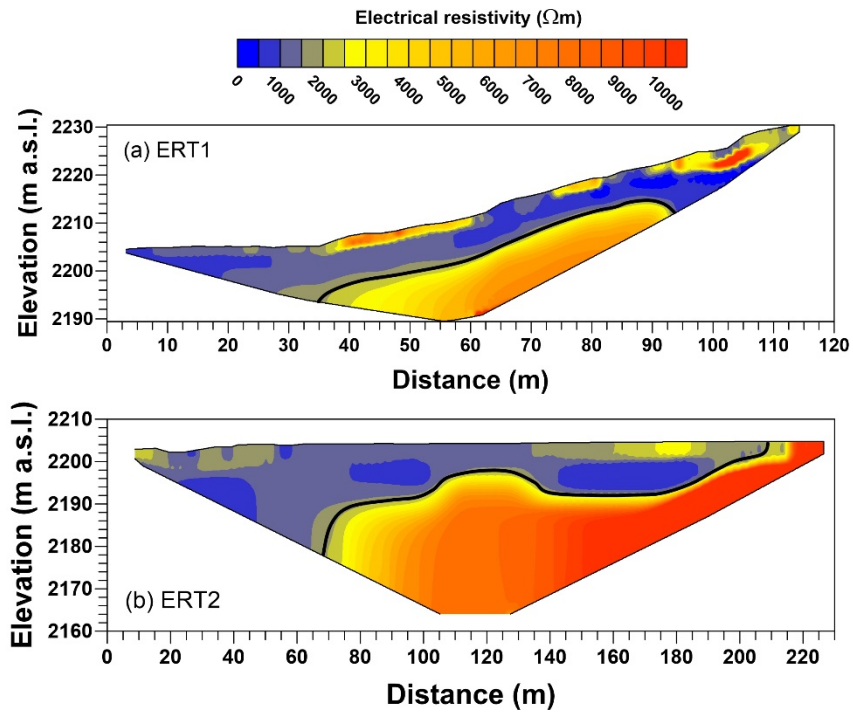
**Figure 6.** Vertical, two-dimensional electrical-resistivity-tomography (ERT) cross sections of profiles (a) ERT1 and (b) ERT2 collected in the sampling zone of Griessfirn (GRF) glacier forefield. Solid black lines indicate the approximate location of the interface between unconsolidated sediment and the bedrock underneath. Lines were omitted at locations where the sediment-rock interface was too deep to be detected.
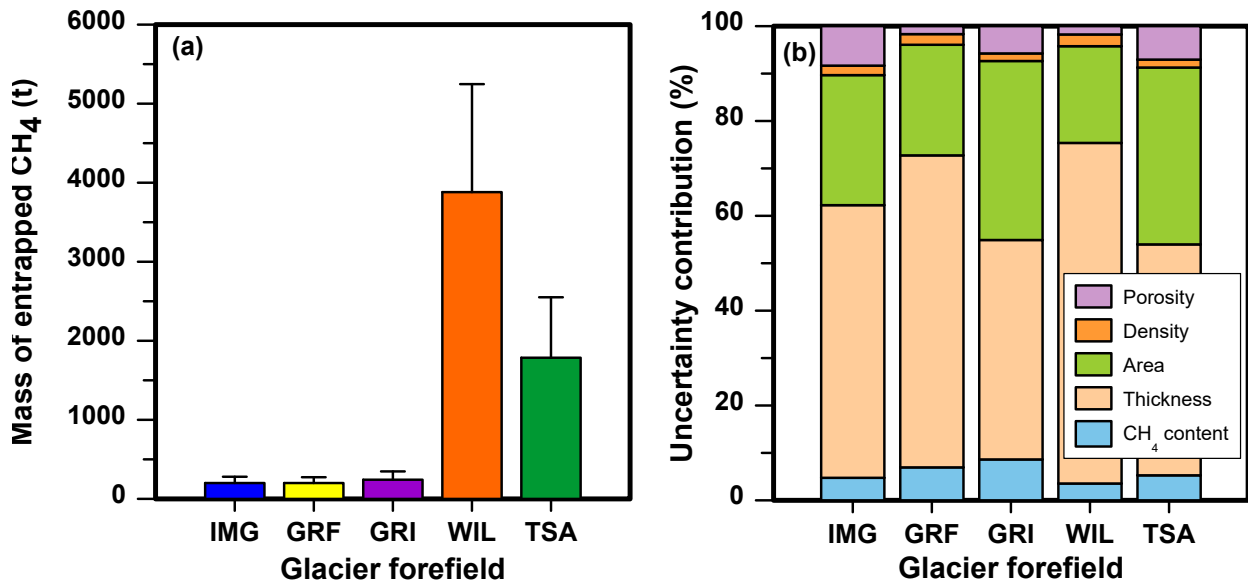
**Figure 7.** a) Estimated mass of CH₄ entrapped in sediments of Im Griess (IMG), Griessfirn (GRF), Griessen (GRI), Wildstrubel (WIL), and Tsanfleuron (TSA) glacier forefields. b) Contribution of sediment-entrapped CH₄ contents, sediment thickness and area, sediment-particle density, and total porosity to total uncertainties in the estimation of the mass of sediment-entrapped CH₄ (error bars in a)) for each of the five glacier forefields.

**Tables**

**Table 1.** Mean values and uncertainties for sediment-entrapped $CH_4$ content, sediment thickness, sediment-covered area, sediment mass, and estimated mass of entrapped $CH_4$ in three different landforms of the Griessfirn (GRF) glacier-forefield sampling zone.

| Landform | Entrapped $CH_4$ content ($\mu g\ CH_4\ g^{-1}$ d.w.) | Sediment thickness (m) | Sediment-covered area ($m^2$) | Sediment mass (t sed.) | Entrapped $CH_4$ mass (t $CH_4$) |
|---|---|---|---|---|---|
| | $\overline{C}_{CH4} \pm \sigma_{\overline{C}_{CH4}}$ [a] | $\overline{T}_{sed} \pm \sigma_{\overline{T}_{sed}}$ | $\overline{A}_{sed} \pm \sigma_{\overline{A}_{sed}}$ | $\overline{m}_{sed} \pm \sigma_{\overline{m}_{sed}}$ | $\overline{m}_{CH4} \pm \sigma_{\overline{m}_{CH4}}$ |
| Floodplain | $6.37 \pm 0.55$ | $11.8 \pm 3.0$ | $2.07 \times 10^4 \pm 2.0 \times 10^2$ | $3.84 \times 10^5 \pm 1.0 \times 10^5$ | $2.4 \pm 0.7$ |
| Terrace | $4.72 \pm 0.97$ | $12.5 \pm 4.0$ | $2.06 \times 10^4 \pm 2.0 \times 10^2$ | $4.04 \times 10^5 \pm 1.3 \times 10^5$ | $1.9 \pm 0.7$ |
| Sandhill | $5.04 \pm 0.78$ | $6.4 \pm 3.2$ | $1.05 \times 10^5 \pm 1.0 \times 10^3$ | $1.06 \times 10^6 \pm 5.4 \times 10^5$ | $5.4 \pm 2.8$ |
| | | | | | $9.7 \pm 3.0$ [b] |
| Combined | $5.38 \pm 0.49$ | $10.2 \pm 3.0$ | $1.47 \times 10^5 \pm 1.4 \times 10^3$ | $2.36 \times 10^6 \pm 7.1 \times 10^5$ | $12.7 \pm 4.0$ [c] |

[a] standard error of the mean (SE).

[b] calculated by adding up estimated mass of entrapped $CH_4$ from each landform.

[c] calculated using average values for entrapped $CH_4$ contents, sediment thickness, and sediment-covered area.

**Table 2.** Mean values and uncertainties of sediment-entrapped $CH_4$ content, sediment-covered area, and total inter-particle sediment porosity for Im Griess (IMG), Griessfirn (GRF), Griessen (GRI), Wildstrubel (WIL), and Tsanfleuron (TSA) glacier forefields located within the Helvetic Nappes of Switzerland. Also listed are individual nappes and major geological formations, from which glacier-forefield sediments are derived.

| Glacier forefield | Entrapped $CH_4$ content ($\mu g\ CH_4\ g^{-1}$ d.w.) | Sediment-covered area ($km^2$) | Sediment porosity[a] (-) | Sediment origin[b] | |
|---|---|---|---|---|---|
| | $\overline{C}_{CH4} \pm \sigma_{\overline{C}_{CH4}}$ [c] | $\overline{A}_{sed} \pm \sigma_{\overline{A}_{sed}}$ | $\overline{\theta}_{t,sed} \pm \sigma_{\overline{\theta}_{t,sed}}$ | Nappes | Geological formations[d] |
| IMG | $6.51 \pm 0.56$ | $2.03 \pm 0.42$ | $0.44 \pm 0.05$ | Kammlistock | Quinten, Schrattenkalk, Stad, Zementstein |
| GRF | $5.59 \pm 0.54$ | $2.27 \pm 0.40$ | $0.42 \pm 0.02$ | Kammlistock Griessstock | Betlis, Helvetic Siliceous Limestone, Öhrli, Quinten, Zementstein |
| GRI | $7.03 \pm 0.91$ | $2.04 \pm 0.55$ | $0.38 \pm 0.04$ | Axen | Bommerstein, Hochstollen, Quinten |
| WIL | $39.41 \pm 2.62$ | $6.35 \pm 1.01$ | $0.43 \pm 0.02$ | Wildhorn Doldenhorn | Garschella, Öhrli, Quinten, Schilt, Schrattenkalk, Seewen, Tierwis |
| TSA | $33.74 \pm 3.31$ | $3.48 \pm 0.91$ | $0.44 \pm 0.05$ | Wildhorn Diablerets | Betlis, Helvetic Siliceous Limestone, Öhrli,Schrattenkalk, Tierwis, Tsanfleuron Member, Pierredar |

 [a] adopted from Nauer et al. (2012).

[b] information obtained from the Geological Atlas of Switzerland 1:25.000 (online at maps.geo.admin.ch), Swiss Federal Office of Topography (swisstopo).

[c] standard error of the mean (SE).

[d] in alphabetical order.

765 **Table 3.** Data used for upscaling the mass of sediment-entrapped $CH_4$ from five sampled glacier forefields (Im Griess (IMG), Griessfirn (GRF), Griessen (GRI), Wildstrubel (WIL), and Tsanfleuron (TSA)) to all calcareous glacier-forefields in Switzerland.

| Parameter | Value | Data source |
|---|---|---|
| Total Alpine area in Switzerland | $2.29 \times 10^4 \pm 504$ km$^2$ | Tectonic Map of Switzerland 1:500.000 (swisstopo) |
| Area of calcareous bedrock | $1.25 \times 10^4 \pm 275$ km$^2$ | Tectonic Map of Switzerland 1:500.000 (swisstopo) |
| Total glaciated area in 1850 | $1.62 \times 10^3 \pm 36$ km$^2$ | Zemp et al. (2008) |
| Total glaciated area in 2010 | $9.44 \times 10^2 \pm 21$ km$^2$ | Fischer et al. (2014) |
| Mean entrapped $CH_4$ content, $\overline{C}_{CH4}$ | $18.5 \pm 4.4$ µg $CH_4$ g$^{-1}$ d.w. | Mean of averages for five glacier forefields |
| Mean sediment thickness, $\overline{T}_{sed}$ | $10.0 \pm 3.0$ m | Measurements in GRF glacier forefield |
| Mean sediment-particle density, $\overline{\rho}_{sed}$ | $2.71 \pm 0.15$ g cm$^{-3}$ | Daly (1935) |
| Mean inter-particle sed. porosity, $\overline{\theta}_{t,sed}$ | $0.44 \pm 0.05$ | Derived from data of Nauer et al. (2012) |
| Mass of sediment-entrapped $CH_4$, $\overline{m}_{CH4}$ | $1.04 \times 10^5 \pm 3.7 \times 10^4$ t $CH_4$ | Eq. (1), this manuscript |